Available online at www.sciencedirect.com
ScienceDirect
Comput. Methods Appl. Mech. Engrg. 370 (2020) 113263
Computer methods in applied mechanics and engineering
www.elsevier.com/locate/cma

Inverse band gap design of elastic metamaterials for P and SV wave control

Heedong Goh[a], Loukas F. Kallivokas[a,b,*]

[a] *Department of Civil, Architectural and Environmental Engineering, The University of Texas at Austin, Austin, TX 78712, United States of America*

[b] *Oden Institute for Computational Engineering and Sciences, The University of Texas at Austin, Austin, TX 78712, United States of America*

Received 28 March 2020; received in revised form 28 June 2020; accepted 30 June 2020
Available online xxxx

Abstract

We describe a systematic approach for engineering the dispersive properties of elastic metamaterials in order to band-gap, at user-defined frequency ranges, the propagation of elastic waves, accounting simultaneously for both P and SV waves. To this end, we focus on the inverse design of a metamaterial's unit cell, and cast the design problem as an optimization problem, driven by the desired band gap, and constrained only by the cell's dispersive characteristics; the latter are expressed in terms of the Floquet–Bloch eigenvalue problem. Numerical results in the time-domain, using metamaterial assemblies with only narrow periodicity, demonstrate that the engineered metamaterial attains the desired behavior. Extensions to wave steering, shielding, and other wave-control applications, follow naturally.

Keywords: Metamaterial; Inverse design; Elastodynamics; Band gap; Group velocity; Dispersion engineering

1. Introduction

Fueled by recent advances in solid state physics, photonics, and phononics, dispersion engineering refers to the emerging field of engineering the properties of materials in order to achieve user-defined behavior, often uncommon in nature (thus giving rise to the metamaterial designation of such materials), which, in the context of wave propagation, would allow for novel ways of wave motion control. To attain the desired behavior, the materials need not necessarily be engineered *ab initio*; instead, for example, one could engineer the spatial arrangement of real materials in periodic (or even aperiodic) assemblies, in a manner that would then endow the assembly with the target dispersive behavior. In this way, wave-steering [1], wave-control [2], cloaking [3–5], band-gapping [6], lensing [7,8], and other wave-control effects become possible.

To date, engineering the dispersive behavior has been attempted mostly on an *ad hoc* basis, and primarily in the context of acoustics or electromagnetics, which enjoy the benefit of a single wave type/wave velocity. By contrast, in elastodynamics, the presence of two distinct wave types turns the engineering of the medium's dispersive

* Corresponding author at: Department of Civil, Architectural and Environmental Engineering, The University of Texas at Austin, Austin, TX 78712, United States of America.
E-mail addresses: heedong.goh@utexas.edu (H. Goh), loukas@mail.utexas.edu (L.F. Kallivokas).

https://doi.org/10.1016/j.cma.2020.113263

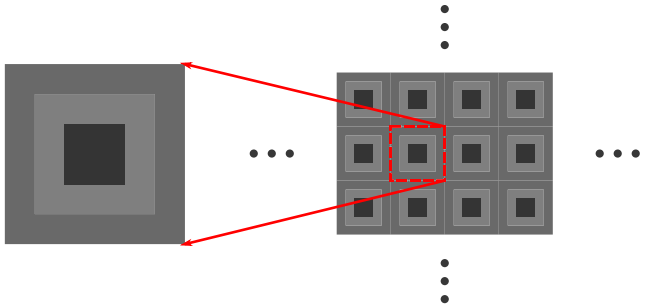

Fig. 1. The unit cell and the metamaterial assembly consisting of periodically arranged heterogeneous unit cells.

characteristics into a particularly challenging task. There are at least two paths to engineering the dispersive behavior: either by topological optimization or by engineering the material composition, or both. Thus far, the few systematic approaches that have been pursued are based almost exclusively on topological optimization: classified by design objective, examples include the works reported in [9–12] for band gap design, in [13,14] for anomalous reflections or refractions, in [15–18] for auxetic or hyperbolic metamaterials, in [19,20] for energy dissipation, and in [21,22] for wave amplitude control.

Engineering material behavior, based on user-defined performance metrics, is, fundamentally, an inverse medium problem, and, therefore, it can be treated using established mathematical approaches for inversion. Here, we build upon recent advances in engineering metamaterials for band-gapping scalar waves (single wave type) [23,24], to the all important and more challenging case of vector waves (two wave types). The goal is to be able to intercept propagating waves with suitably engineered metabarriers in order to arrest (filter) the propagation of elastic waves at user-defined frequency ranges (the band gaps). While the discussion herein is driven by band gaps, other wave control objectives can be similarly pursued by appropriately adapting the developed framework.

2. Preliminaries

Let us assume that the metamaterial, whose dispersive behavior we intend to engineer, consists of identical, periodically distributed, unit cells (Fig. 1): due to the periodicity, it is sufficient to engineer the unit cell in order to endow the metamaterial with the desired target behavior. The dispersive behavior of the unit cell is completely defined by the associated eigenvalue problem (EP), cast over the unit cell and subject to periodic boundary conditions. While the EP captures the unit cell's dispersive characteristics, it cannot be readily manipulated to meet a specific design goal: instead, we use the EP to extract the band structure, i.e., the dispersion curves/surfaces associated with the irreducible Brillouin zone (IBZ). The IBZ affords us the necessary flexibility to accommodate wave-control design goals, and in particular when targeting directionality constraints. We highlight next the steps leading to the unit-cell design informed by the IBZ: in short, *dispersion engineering design goals* are first translated to specific *group velocity design profiles*, which are, in turn, shown to uniquely depend on the characteristics of the unit cell's *EP and IBZ.*

2.1. The eigenvalue problem for elastic waves in periodic media

In the frequency domain, the propagation of elastic waves in a heterogeneous domain is described by Navier's equations:

$$\mathbf{0} = \operatorname{div} \underline{\underline{\mathbf{C}}}(\boldsymbol{x}) \left[\operatorname{grad} \mathbf{U}(\boldsymbol{x})\right] + \rho(\boldsymbol{x})\, \omega^2 \mathbf{U}(\boldsymbol{x}), \quad \boldsymbol{x} \in \mathbb{R}^{N_\mathrm{d}}, \tag{1}$$

where N_d denotes the order of the spatial dimensionality, $\mathbf{U}(\boldsymbol{x})$ is the displacement vector, ω is the circular frequency, $\rho(\boldsymbol{x})$ is mass density, and $\underline{\underline{\mathbf{C}}}(\boldsymbol{x})$ is the elasticity tensor. We use regular font to denote scalars, and boldfaced font for vectors, matrices, and first-rank tensors; a single underline is used for second-rank tensors; and a double underline is used for fourth-rank tensors. The elasticity tensor $\underline{\underline{\mathbf{C}}}$ for a linear isotropic medium reads:

$$\underline{\underline{\mathbf{C}}}(\boldsymbol{x})[\ ] = \mu(\boldsymbol{x})[\ ] + \mu(\boldsymbol{x})[\ ]^{\mathsf{T}} + \lambda(\boldsymbol{x}) \operatorname{tr}[\ ] \underline{\mathbf{I}}, \tag{2}$$

where $\lambda(\boldsymbol{x})$ and $\mu(\boldsymbol{x})$ are the Lamé parameters, $\underline{\mathbf{I}}$ is the identity tensor and $[\ ]^{\mathsf{T}}$ denotes the transpose of the subtended quantity. The problem implied by (1) becomes periodic when the material properties are periodic, i.e., when $\forall \boldsymbol{x} \in \mathbb{R}^{N_\mathrm{d}}$ and $\forall m_i \in \mathbb{Z}$,

$$\lambda(\boldsymbol{x}) = \lambda\left(\boldsymbol{x} + \sum_{i=1}^{N_\mathrm{d}} m_i \mathbf{p}_i\right), \tag{3a}$$

$$\mu(\boldsymbol{x}) = \mu\left(\boldsymbol{x} + \sum_{i=1}^{N_\mathrm{d}} m_i \mathbf{p}_i\right), \quad \text{and} \tag{3b}$$

$$\rho(\boldsymbol{x}) = \rho\left(\boldsymbol{x} + \sum_{i=1}^{N_\mathrm{d}} m_i \mathbf{p}_i\right). \tag{3c}$$

In the above, $\mathbf{p}_i \in \mathbb{R}^{N_\mathrm{d}}$ is the primitive vector that defines the periodicity in the ith spatial direction. Then, the *Floquet–Bloch theorem* [25] provides the general solution of the periodic problem as:

$$\mathbf{U}(\boldsymbol{x}) = e^{\mathrm{i}\mathbf{k}\cdot\boldsymbol{x}}\mathbf{u}(\boldsymbol{x}), \tag{4}$$

where the displacement-like quantity $\mathbf{u}(\boldsymbol{x})$ is periodic with the same periodicity of the original problem, and $\mathbf{k}$ denotes the Floquet–Bloch wavevector. Substituting (4) into the Navier equation (1), yields the *Floquet–Bloch EP*. In weak form, the EP reads: given $\omega \in \mathbb{R}$ and $\mathbf{d} \in \mathbb{R}^{N_\mathrm{d}}$, find $k \in \mathbb{C}$ and $\mathbf{u} \in \mathcal{V}^{N_\mathrm{d}} \setminus \{\mathbf{0}\}$ such that

$$P(k)(\mathbf{v},\mathbf{u}) \equiv a_0(\mathbf{v},\mathbf{u}) + k a_1(\mathbf{v},\mathbf{u}) + k^2 a_2(\mathbf{v},\mathbf{u}) = 0, \quad \forall \mathbf{v} \in \mathcal{V}^{N_\mathrm{d}}, \tag{5}$$

where

$$\mathcal{V} = \left\{ w \in H^1(\Omega_{\mathrm{cell}}) \,|\, w(\boldsymbol{x}) = w\left(\boldsymbol{x} + \sum_{i=1}^{N_\mathrm{d}} m_i \mathbf{p}_i\right) \ \forall \boldsymbol{x} \in \partial\Omega_{\mathrm{cell}} \right\}, \tag{6a}$$

$$a_0(\mathbf{v},\mathbf{u}) = \int_{\Omega_{\mathrm{cell}}} \left\{ \operatorname{grad}\overline{\mathbf{v}} : \underline{\underline{\mathbf{C}}}\left[\operatorname{grad}\mathbf{u}\right] - \overline{\mathbf{v}} \cdot \omega^2 \rho\, \mathbf{u} \right\} d\Omega, \tag{6b}$$

$$a_1(\mathbf{v},\mathbf{u}) = \mathrm{i}\int_{\Omega_{\mathrm{cell}}} \left\{ \operatorname{grad}\overline{\mathbf{v}} : \underline{\underline{\mathbf{C}}}\left[\mathbf{u}\otimes\mathbf{d}\right] - (\overline{\mathbf{v}}\otimes\mathbf{d}) : \underline{\underline{\mathbf{C}}}\left[\operatorname{grad}\mathbf{u}\right] \right\} d\Omega, \quad \text{and} \tag{6c}$$

$$a_2(\mathbf{v},\mathbf{u}) = \int_{\Omega_{\mathrm{cell}}} (\overline{\mathbf{v}}\otimes\mathbf{d}) : \underline{\underline{\mathbf{C}}}\left[\mathbf{u}\otimes\mathbf{d}\right] d\Omega. \tag{6d}$$

In the above, Ω_{cell} is the domain of a unit cell, $\mathbf{v}$ is a test function, an overline $\overline{(\ )}$ denotes a complex-conjugate of the subtended quantity, $(:)$ denotes double contraction, $\otimes$ denotes tensor product, and $\mathbf{d}$ is a direction of interest such that $\mathbf{k} = k\mathbf{d}$, with $|\mathbf{d}| = 1$.

We prefer to drive the unit cell's design using the quadratic EP (5), cast in terms of the wavenumber k, instead of the more common choice of the linear EP (cast in terms of ω^2), since, as discussed in [23], the quadratic EP provides a direct, quantitative, description of the band gaps, whereas the linear EP can only offer an indirect description. Thus, given a (real-valued) circular frequency ω, we use (5) to find the complex-valued wavenumbers (wavevectors) k ($\mathbf{k}$): the set of all dispersion curves/surfaces relating ω to $\mathbf{k}$ forms the *band structure* of the unit cell. We note that the Floquet–Bloch wavevector $\mathbf{k}$ is periodic in the wavevector space (or reciprocal space); the periodicity in the reciprocal space is captured by the reciprocal primitive vector $\mathbf{q}_i$, which is related to the physical space's primitive vector $\mathbf{p}_i$ via $\mathbf{p}_i \cdot \mathbf{q}_j = 2\pi\delta_{ij}$, with δ_{ij} denoting the Kronecker delta. Similarly, the dispersion curves of a periodic problem are also periodic in the wavevector space with periodicity equal to that of the primitive vector $\mathbf{q}_i$.

To study the band structure we turn to the unit cell (or Wigner–Seitz cell) in the reciprocal space: the Wigner–Seitz cell defines the Brillouin zone, which is, effectively, the (periodic) trace of the dispersion curves in the wavevector space. The dispersion curves have symmetries that allow a further reduction of the Brillouin zone to the, so-called, *irreducible Brillouin zone* (IBZ), which is delineated off of the Brillouin zone while ensuring that no information is lost. Practically, dispersion curves are often plotted over only the *high-symmetry lines*, which are the edges of the IBZ. For example, a square unit cell in the physical space has a square Wigner–Seitz cell in the reciprocal/wavevector space (i.e., a square Brillouin zone), which, upon reduction, results in a triangular IBZ (Fig. 2). The vertices of the triangular IBZ are denoted by Γ, X, and M, and the three high-symmetry lines are Γ-X, Γ-M, and X-M. In this paper, we plot dispersion curves for wavevectors corresponding only to the propagating states to avoid congesting the plots.

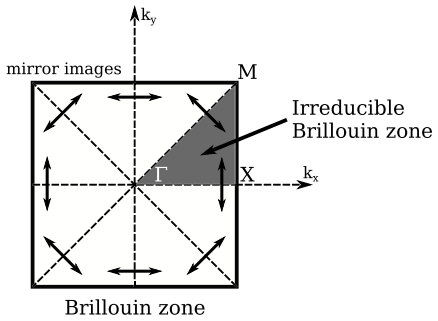

Fig. 2. The Brillouin zone and the IBZ of a square unit cell in wavevector space.

We remark that to compute the band structure on the high-symmetry lines that do not connect back to the origin Γ, e.g., X-M in Fig. 2, an offset direction $\mathbf{d}_o$ is required, such that $\mathbf{k} = k\mathbf{d} + \mathbf{d}_o$: the associated EP with an offset direction is given in Appendix A.

2.2. Group velocity, energy velocity, and the band gap

We are interested in engineering the unit cell to exhibit user-defined dispersive behavior, and in particular, to adhere to a user-prescribed group velocity profile. Band gaps are only a particular case of a group velocity profile. Specifically, a band gap is a frequency range $\mathcal{G}$ for which there are no propagating states: at the band gap frequencies, the Floquet–Bloch wavenumbers are complex-valued with nonzero imaginary parts ($\mathrm{Im}\{k\} \neq 0$, $\forall \omega \in \mathcal{G}$), whereas outside the gap the wavenumbers are purely real-valued ($k \in \mathbb{R}$, $\forall \omega \notin \mathcal{G}$). As will be discussed, band gaps arise when the group velocity vanishes. Then, to set up the inverse design problem, it is necessary to relate the group velocity to the unit-cell EP.

The group velocity $\mathbf{v}_g$ is defined as [26]:

$$\mathbf{v}_g = \mathrm{Re}\left\{\mathrm{grad}_k \omega\right\}, \tag{7}$$

while the directional group velocity along $\mathbf{d}$ is:

$$v_g = \mathbf{v}_g \cdot \mathbf{d} = \mathrm{Re}\left\{\frac{\partial \omega}{\partial k}\right\}. \tag{8}$$

To relate the group velocity to the EP, we differentiate (5) with respect to k, i.e.,

$$\begin{aligned} 0 &= \frac{\partial}{\partial k} P(k)(\mathbf{u}, \mathbf{u}) \\ &= 2\omega \frac{\partial \omega}{\partial k} a_{0,2}(\mathbf{u}, \mathbf{u}) + a_1(\mathbf{u}, \mathbf{u}) + 2k a_2(\mathbf{u}, \mathbf{u}) + 2\mathrm{Re}\left\{P(k)\left(\frac{\partial \mathbf{u}}{\partial k}, \mathbf{u}\right)\right\}. \end{aligned} \tag{9}$$

In the above, the last term vanishes, assuming that $\partial \mathbf{u}/\partial k \in \mathcal{V}^{N_\mathrm{d}}$. Then, by taking the real part of the remainder of (9), while considering (8), yields:

$$v_g = -\frac{a_1(\mathbf{u}, \mathbf{u}) + 2\mathrm{Re}\{k\} a_2(\mathbf{u}, \mathbf{u})}{2\,\omega\, a_{0,2}(\mathbf{u}, \mathbf{u})}, \tag{10}$$

where

$$a_{0,2}(\mathbf{v}, \mathbf{u}) = -\int_{\Omega_\mathrm{cell}} \overline{\mathbf{v}} \cdot \rho\, \mathbf{u}\, d\Omega. \tag{11}$$

Expression (10) is the sought relation between the (directional) group velocity v_g and the eigenpair $(\mathbf{u}, k)$ of the Floquet–Bloch unit-cell EP: it can be viewed as the elastodynamic equivalent of the Hellmann–Feynman theorem in quantum mechanics, and it is a key element in the inverse unit-cell design problem, since, by specifying the left-hand-side of (10), it is possible to invert for the unit-cell properties associated with the eigenpair $(\mathbf{u}, k)$ that

appears on the right-hand-side of (10). If, for example, it is of interest to realize a band gap along any particular direction $\mathbf{d}$, then the directional group velocity must vanish [24], i.e.,

$$v_g = 0, \quad \forall\, \omega \in \mathcal{G}, \tag{12}$$

or, equivalently, by virtue of (10):

$$a_1(\mathbf{u},\mathbf{u}) + 2\mathrm{Re}\{k\}\, a_2(\mathbf{u},\mathbf{u}) = 0. \tag{13}$$

We note that the group velocity is defined with respect to the Floquet–Bloch wavevector corresponding to the ansatz (4), which differs from the usual definition for plane waves, and obscures the physical interpretation of the group velocity. However, as it was first shown in [27] for Floquet–Bloch wavenumbers k corresponding to propagating states ($k \in \mathbb{R}$), the group velocity is identical to the energy velocity, i.e.,

$$v_g = v_e, \quad \forall\, \omega \notin \mathcal{G}, \tag{14}$$

where $v_e = \mathbf{v}_e \cdot \mathbf{d}$ is the directional energy velocity. Here, we show again the velocity equivalence relation for Floquet–Bloch wavenumbers, following a slightly different path than the one in [27], which has the benefit of explicitly relating the energy velocity to the Floquet–Bloch eigenpair and the sesquilinear forms of the eigenvalue problem, as was earlier done for the group velocity in (10). Accordingly, the energy velocity $\mathbf{v}_e$ for a time-harmonic elastic wave is defined as [28,29]:

$$\mathbf{v}_e = \frac{\mathrm{Re}\{\langle \mathbf{F} \rangle\}}{\langle \mathcal{E} \rangle}, \tag{15}$$

where $\langle\ \rangle$ denotes spatial average, $\mathbf{F}$ is the time-averaged Umov–Poynting vector, and $\mathcal{E}$ is time-averaged energy [28]. The time-averaged Umov–Poynting vector $\mathbf{F}$ and time-averaged energy $\mathcal{E}$ (assuming an $e^{-\mathrm{i}\omega t}$ harmonic factor) are defined as:

$$\mathbf{F} = -\frac{1}{2}\underline{\boldsymbol{\tau}}^{\mathsf{T}}\overline{(-\mathrm{i}\omega)\,\mathbf{U}}, \quad \text{and} \tag{16}$$

$$\mathcal{E} = U + K = \frac{1}{4}\mathrm{Re}\left\{\overline{\underline{\varepsilon}} : \underline{\boldsymbol{\tau}}\right\} + \frac{1}{4}\rho\,\overline{(-\mathrm{i}\omega)\,\mathbf{U}} \cdot (-\mathrm{i}\omega)\,\mathbf{U}, \tag{17}$$

where U is time-averaged strain energy, K is time-averaged kinetic energy, $\underline{\boldsymbol{\tau}}$ is a stress tensor, $\underline{\varepsilon}$ is a strain tensor. Then, the time-averaged Umov–Poynting vector in the direction $\mathbf{d}$ is:

$$\begin{aligned}
\mathbf{F}\cdot\mathbf{d} &= -\frac{1}{2}\left(\underline{\boldsymbol{\tau}}^{\mathsf{T}}\overline{(-\mathrm{i}\omega)\,\mathbf{U}}\right)\cdot\mathbf{d} \\
&= -\frac{1}{2}\underline{\boldsymbol{\tau}} : \left(\overline{(-\mathrm{i}\omega)\,\mathbf{U}} \otimes \mathbf{d}\right) \\
&= -\frac{1}{2}\underline{\underline{\mathbf{C}}}\left[\mathrm{grad}\,\mathbf{U}\right] : \left(\mathrm{i}\omega\overline{\mathbf{U}} \otimes \mathbf{d}\right) \\
&= -\frac{1}{2}\underline{\underline{\mathbf{C}}}\left[\mathrm{grad}\,\mathbf{u} + \mathbf{u}\otimes\mathrm{i}\mathbf{k}\right]e^{\mathrm{i}\mathbf{k}\cdot\boldsymbol{x}} : \left(\mathrm{i}\omega\overline{\mathbf{u}}e^{-\mathrm{i}\mathbf{k}\cdot\boldsymbol{x}} \otimes \mathbf{d}\right) \\
&= -\frac{1}{2}\mathrm{i}\omega\,(\overline{\mathbf{u}}\otimes\mathbf{d}) : \underline{\underline{\mathbf{C}}}\left[\mathrm{grad}\,\mathbf{u}\right] + \frac{1}{2}\omega k\,(\overline{\mathbf{u}}\otimes\mathbf{d}) : \underline{\underline{\mathbf{C}}}\left[\mathbf{u}\otimes\mathbf{d}\right].
\end{aligned} \tag{18}$$

In the above, the identity $\left(\underline{\mathbf{A}}^{\mathsf{T}}\mathbf{a}\right)\cdot\mathbf{b} = \mathrm{tr}\left(\underline{\mathbf{A}}^{\mathsf{T}}\mathbf{a}\otimes\mathbf{b}\right) = \underline{\mathbf{A}} : (\mathbf{a}\otimes\mathbf{b})$ is used [30]. Taking the spatial average of the real part of (18), yields:

$$\begin{aligned}
|\Omega_{\mathrm{cell}}|\,\mathrm{Re}\{\langle\mathbf{F}\cdot\mathbf{d}\rangle\} &= \frac{1}{2}\omega\mathrm{Re}\left\{-\mathrm{i}\int_{\Omega_{\mathrm{cell}}}(\overline{\mathbf{u}}\otimes\mathbf{d}) : \underline{\underline{\mathbf{C}}}\left[\mathrm{grad}\,\mathbf{u}\right]d\Omega\right\} + \frac{1}{2}\omega\mathrm{Re}\left\{k\int_{\Omega_{\mathrm{cell}}}(\overline{\mathbf{u}}\otimes\mathbf{d}) : \underline{\underline{\mathbf{C}}}\left[\mathbf{u}\otimes\mathbf{d}\right]d\Omega\right\} \\
&= \frac{1}{4}\omega\mathrm{Re}\left\{\mathrm{i}\int_{\Omega_{\mathrm{cell}}}\left\{\underline{\underline{\mathbf{C}}}\left[\mathrm{grad}\,\overline{\mathbf{u}}\right] : (\mathbf{u}\otimes\mathbf{d}) - (\overline{\mathbf{u}}\otimes\mathbf{d}) : \underline{\underline{\mathbf{C}}}\left[\mathrm{grad}\,\mathbf{u}\right]\right\}d\Omega\right\} \\
&\quad + \frac{1}{2}\omega\mathrm{Re}\left\{k\int_{\Omega_{\mathrm{cell}}}(\overline{\mathbf{u}}\otimes\mathbf{d}) : \underline{\underline{\mathbf{C}}}\left[\mathbf{u}\otimes\mathbf{d}\right]d\Omega\right\} \\
&= \frac{1}{4}\omega\left[a_1(\mathbf{u},\mathbf{u}) + 2\mathrm{Re}\{k\}\,a_2(\mathbf{u},\mathbf{u})\right],
\end{aligned} \tag{19}$$

where $|\Omega_{\text{cell}}|$ is the area of the unit cell. Next, we compute the time-averaged energy by

$$\begin{aligned}
\mathcal{E} &= U + K \\
&= \frac{1}{4}\text{Re}\left\{\underline{\boldsymbol{\tau}} : \overline{\underline{\boldsymbol{\varepsilon}}}\right\} + \frac{1}{4}\rho\,(-\text{i}\omega)\,\mathbf{U}\cdot\overline{(-\text{i}\omega)\,\mathbf{U}} \\
&= \frac{1}{4}\text{Re}\left\{\underline{\underline{\mathbf{C}}}\left[\text{grad}\,\mathbf{U}\right] : \overline{\text{grad}\,\mathbf{U}}\right\} + \frac{1}{4}\rho\,\omega^2\mathbf{U}\cdot\overline{\mathbf{U}} \\
&= \frac{1}{4}\text{Re}\left\{\underline{\underline{\mathbf{C}}}\left[\text{grad}\,\mathbf{u} + \mathbf{u}\otimes\text{i}\mathbf{k}\right] : (\text{grad}\,\overline{\mathbf{u}} - \overline{\mathbf{u}}\otimes\text{i}\mathbf{k})\right\} + \frac{1}{4}\rho\,\omega^2\mathbf{u}\cdot\overline{\mathbf{u}} \\
&= \frac{1}{4}\text{Re}\left\{\text{grad}\,\overline{\mathbf{u}} : \underline{\underline{\mathbf{C}}}\left[\text{grad}\,\mathbf{u}\right]\right\} + \frac{1}{4}\text{Re}\left\{\text{i}k\left(\text{grad}\,\overline{\mathbf{u}} : \underline{\underline{\mathbf{C}}}\left[\mathbf{u}\otimes\mathbf{d}\right] - (\overline{\mathbf{u}}\otimes\mathbf{d}) : \underline{\underline{\mathbf{C}}}\left[\text{grad}\,\mathbf{u}\right]\right)\right\} \\
&\quad + \frac{1}{4}\text{Re}\left\{k^2\,(\overline{\mathbf{u}}\otimes\mathbf{d}) : \underline{\underline{\mathbf{C}}}\left[\mathbf{u}\otimes\mathbf{d}\right]\right\} + \frac{1}{4}\rho\,\omega^2\mathbf{u}\cdot\overline{\mathbf{u}}.
\end{aligned} \tag{20}$$

The energy's spatial average reads:

$$\begin{aligned}
|\Omega_{\text{cell}}|\,\langle\mathcal{E}\rangle &= \frac{1}{4}\text{Re}\left\{\int_{\Omega_{\text{cell}}} \text{grad}\,\overline{\mathbf{u}} : \underline{\underline{\mathbf{C}}}\left[\text{grad}\,\mathbf{u}\right] d\Omega\right\} \\
&\quad + \frac{1}{4}\text{Re}\left\{k\int_{\Omega_{\text{cell}}} \text{i}\left\{\text{grad}\,\overline{\mathbf{u}} : \underline{\underline{\mathbf{C}}}\left[\mathbf{u}\otimes\mathbf{d}\right] - (\overline{\mathbf{u}}\otimes\mathbf{d}) : \underline{\underline{\mathbf{C}}}\left[\text{grad}\,\mathbf{u}\right]\right\} d\Omega\right\} \\
&\quad + \frac{1}{4}\text{Re}\left\{k^2\int_{\Omega_{\text{cell}}} (\overline{\mathbf{u}}\otimes\mathbf{d}) : \underline{\underline{\mathbf{C}}}\left[\mathbf{u}\otimes\mathbf{d}\right] d\Omega\right\} + \frac{1}{4}\int_{\Omega_{\text{cell}}} \rho\,\omega^2\mathbf{u}\cdot\overline{\mathbf{u}} d\Omega \\
&= \frac{1}{4}\text{Re}\left\{P\,(k)\,(\mathbf{u},\mathbf{u})\right\} + \frac{1}{2}\int_{\Omega_{\text{cell}}} \rho\,\omega^2\mathbf{u}\cdot\overline{\mathbf{u}} d\Omega \\
&= -\frac{1}{2}\omega^2 a_{0,2}\,(\mathbf{u},\mathbf{u})\,.
\end{aligned} \tag{21}$$

Substituting (19) and (21) into (15), yields

$$v_e = \frac{\text{Re}\left\{\langle\mathbf{F}\cdot\mathbf{d}\rangle\right\}}{\langle\mathcal{E}\rangle} = -\frac{a_1\,(\mathbf{u},\mathbf{u}) + 2\text{Re}\left\{k\right\}a_2\,(\mathbf{u},\mathbf{u})}{2\,\omega\,a_{0,2}\,(\mathbf{u},\mathbf{u})}, \quad \omega \notin \mathcal{G}. \tag{22}$$

This completes the proof and reaffirms the result in [27]: Eq. (22) is identical to (10) and confirms that the group velocity is, for propagating states, physically identical to the energy velocity, while both are cast in terms of the Floquet–Bloch eigenpair.

3. The metamaterial unit-cell design

In general, the unit-cell design is driven by a user-defined group velocity profile: this, for example, could drive designs that allow for slow or fast wave regimes at specific frequency ranges. Moreover, for the applications considered herein, a user-defined band gap is tantamount to requiring that the group velocity vanish within the desired frequency range. We describe next the inverse medium framework that would produce the unit-cell's design parameters, when given a target group velocity profile.

3.1. Dispersion-constrained inverse problem

The design problem is cast as a dispersion-constrained inverse problem, where the Lagrangian L consists of a misfit objective functional M, and of the dispersion constraint E. Accordingly, it reads: given $v_g^m \in \mathbb{R}$, find $\rho \in \mathcal{W}$, $\lambda \in \mathcal{W}$, and $\mu \in \mathcal{W}$ such that

$$\min L\,[\mathbf{u}, k, \mathbf{v}, \xi, \rho, \lambda, \mu]\,, \tag{23}$$

where,

$$L\left[\mathbf{u},k,\mathbf{v},\xi,\rho,\lambda,\mu\right]=M\left[\mathbf{u},k,\rho,\lambda,\mu\right]+E\left[\mathbf{u},k,\mathbf{v},\xi,\rho,\lambda,\mu\right], \tag{24a}$$

$$M\left[\mathbf{u},k,\rho,\lambda,\mu\right]=\sum_{\alpha}^{N_{\text{freq}}}\sum_{\beta}^{N_{\text{dir}}}\sum_{\gamma}^{N_{\text{mode}}}\frac{1}{2}\left(v_{g,\alpha\beta\gamma}-v_{g,\alpha\beta\gamma}^{m}\right)^{2}, \tag{24b}$$

$$E\left[\mathbf{u},k,\mathbf{v},\xi,\rho,\lambda,\mu\right]=\sum_{\alpha}^{N_{\text{freq}}}\sum_{\beta}^{N_{\text{dir}}}\sum_{\gamma}^{N_{\text{mode}}}\left[\text{Re}\left\{P\left(k\right)\left(\mathbf{v},\mathbf{u}\right)\right\}+\frac{\xi}{2}\left\{a_2\left(\mathbf{u},\mathbf{u}\right)-1\right\}\right]_{\alpha\beta\gamma}, \quad \text{and} \tag{24c}$$

$$\mathcal{W}=\left\{w\in H^0\left(\Omega_{\text{cell}}\right)\,|\,w\left(\boldsymbol{x}\right)=w\left(\boldsymbol{x}+\sum_{i=1}^{N_{\text{d}}}m_i\mathbf{p}_i\right)\ \forall\boldsymbol{x}\in\partial\Omega_{\text{cell}}\right\}. \tag{24d}$$

In the above, M is an objective functional defined as the misfit between the target (v_g^m) and the trial (v_g) group velocities, where the latter are computed based on trial unit-cell design parameters. In addition, E is the dispersion constraint, side-imposed in (24a) in terms of the Floquet–Block EP $P(k)$ of (5) and the corresponding orthonormality condition for the eigenfunctions $\mathbf{u}$; $\mathbf{v}$ is the adjoint eigenfunction, and ξ is the adjoint eigenvalue. We note that N_{freq} is the set of the discrete frequencies spanning the target band gap $\mathcal{G}$, N_{dir} are the user-defined directions along which the propagating waves will be band-gaped, and N_{mode} is the number of modes. For an omnidirectional band gap, the set of directions N_{dir} must cover the entire IBZ, or, at a minimum contain all the high-symmetry lines. It should be noted that for each frequency, direction, and mode, a separate EP arises, and thus, the dispersion constraint E consists of $N_{\text{freq}}\times N_{\text{dir}}\times N_{\text{mode}}$ eigenvalue problems: this explains the triple $\alpha\beta\gamma$ subscripting of the EP in (24b), and of the computed $v_{g,\alpha\beta\gamma}$ and prescribed $v_{g,\alpha\beta\gamma}^m$ group velocities, respectively; however, henceforth, we drop the subscripting to reduce notational congestion.

3.2. Solution method

We seek solutions for the design variables of the unconstrained minimization problem (23) by requiring that the first-order optimality conditions be satisfied, i.e., by setting to zero the first-order derivatives of the Lagrangian $(M+E)$ with respect to the state variables ($\mathbf{u}$ and k), adjoint variables ($\mathbf{v}$ and ξ), and design variables (λ, μ, and ρ). The process is iterative: first, we choose a trial solution for the triad of the design variables; then, the derivative of L with respect to the adjoint variables $\mathbf{v}$ and ξ, yields:

State problem: given $\rho\in\mathcal{W}$, $\lambda\in\mathcal{W}$, and $\mu\in\mathcal{W}$, find $\mathbf{u}\in\mathcal{V}^{N_{\text{d}}}\setminus\{\mathbf{0}\}$ and $k\in\mathbb{C}$ such that

$$P\left(k\right)\left(\tilde{\mathbf{v}},\mathbf{u}\right)=0\quad\forall\tilde{\mathbf{v}}\in\mathcal{V}^{N_{\text{d}}}\quad\text{and} \tag{25a}$$

$$\frac{\tilde{\xi}}{2}\left\{a_2\left(\mathbf{u},\mathbf{u}\right)-1\right\}=0\quad\forall\tilde{\xi}\in\mathbb{R}. \tag{25b}$$

Next, we take derivatives of L with respect to the state variables $\mathbf{u}$ and k, which results in the

Adjoint problem: given the solutions to the state problem $\mathbf{u}\in\mathcal{V}^{N_{\text{d}}}\setminus\{\mathbf{0}\}$, and $k\in\mathbb{C}$, and the triad of trial design variables $\rho\in\mathcal{W}$, $\lambda\in\mathcal{W}$, and $\mu\in\mathcal{W}$, find $\mathbf{v}\in\mathcal{V}^{N_{\text{d}}}$ and $\xi\in\mathbb{R}$ such that

$$\begin{aligned}P\left(k\right)\left(\mathbf{v},\tilde{\mathbf{u}}\right)+\xi a_2\left(\mathbf{u},\tilde{\mathbf{u}}\right)=&\frac{a_1\left(\mathbf{u},\tilde{\mathbf{u}}\right)+2\text{Re}\left\{k\right\}a_2\left(\mathbf{u},\tilde{\mathbf{u}}\right)}{\omega\,a_{0,2}\left(\mathbf{u},\mathbf{u}\right)}\left(v_g-v_g^m\right)\\&-\frac{a_1\left(\mathbf{u},\mathbf{u}\right)+2\text{Re}\left\{k\right\}a_2\left(\mathbf{u},\mathbf{u}\right)}{\omega\left[a_{0,2}\left(\mathbf{u},\mathbf{u}\right)\right]^2}a_{0,2}\left(\mathbf{u},\tilde{\mathbf{u}}\right)\left(v_g-v_g^m\right)\quad\forall\tilde{\mathbf{u}}\in\mathcal{V}^{N_{\text{d}}}\quad\text{and}\end{aligned} \tag{26a}$$

$$\tilde{k}a_1\left(\mathbf{v},\mathbf{u}\right)+2k\tilde{k}a_2\left(\mathbf{v},\mathbf{u}\right)=\frac{\tilde{k}a_2\left(\mathbf{u},\mathbf{u}\right)}{\omega\,a_{0,2}\left(\mathbf{u},\mathbf{u}\right)}\left(v_g-v_g^m\right)\quad\forall\tilde{k}\in\mathbb{C}. \tag{26b}$$

Finally, given the state and adjoint solutions, we take derivatives of L with respect to the design variables ρ, λ, and μ to obtain the gradients g_ρ, g_λ, and g_μ, respectively, i.e.,

Gradient of L: given $\mathbf{v} \in \mathcal{V}^{N_\mathrm{d}}$, $\xi \in \mathbb{R}$, $\mathbf{u} \in \mathcal{V}^{N_\mathrm{d}} \setminus \{\mathbf{0}\}$, $k \in \mathbb{C}$, $\rho \in \mathcal{W}$, $\lambda \in \mathcal{W}$, and $\mu \in \mathcal{W}$, there result:

$$\begin{aligned}\int_{\Omega_\mathrm{cell}} \tilde{\rho} g_\rho d\Omega = &\sum_\alpha^{N_\mathrm{freq}} \sum_\beta^{N_\mathrm{dir}} \sum_\gamma^{N_\mathrm{mode}} \left(\frac{a_1(\mathbf{u},\mathbf{u}) + 2\mathrm{Re}\{k\} a_2(\mathbf{u},\mathbf{u})}{2\omega \left[a_{0,2}(\mathbf{u},\mathbf{u})\right]^2} \right) \left(-\int_{\Omega_\mathrm{cell}} \overline{\mathbf{u}} \cdot \tilde{\rho}\mathbf{u} d\Omega \right) \left(v_g - v_g^m\right) \\ &+ \sum_\alpha^{N_\mathrm{freq}} \sum_\beta^{N_\mathrm{dir}} \sum_\gamma^{N_\mathrm{mode}} \mathrm{Re}\left\{ -\int_{\Omega_\mathrm{cell}} \overline{\mathbf{v}} \cdot \tilde{\rho}\, \omega^2 \mathbf{u} d\Omega \right\} \quad \forall \tilde{\rho} \in \mathcal{W}, \end{aligned} \tag{27a}$$

$$\begin{aligned}\int_{\Omega_\mathrm{cell}} \tilde{\lambda} g_\lambda d\Omega = &\sum_\alpha^{N_\mathrm{freq}} \sum_\beta^{N_\mathrm{dir}} \sum_\gamma^{N_\mathrm{mode}} \left(-\frac{\mathrm{i}\int_{\Omega_\mathrm{cell}} \left\{ \mathrm{grad}\,\overline{\mathbf{u}} : \delta_\lambda \underline{\underline{\mathbf{C}}}[\mathbf{u}\otimes\mathbf{d}] - (\overline{\mathbf{u}}\otimes\mathbf{d}) : \delta_\lambda \underline{\underline{\mathbf{C}}}\left[\mathrm{grad}\,\mathbf{u}\right] \right\} d\Omega}{2\omega a_{0,2}(\mathbf{u},\mathbf{u})} \right. \\ &\left. - \frac{2\mathrm{Re}\{k\} \int_{\Omega_\mathrm{cell}} (\overline{\mathbf{u}}\otimes\mathbf{d}) : \delta_\lambda \underline{\underline{\mathbf{C}}}[\mathbf{u}\otimes\mathbf{d}] d\Omega}{2\omega a_{0,2}(\mathbf{u},\mathbf{u})} \right) \left(v_g - v_g^m\right) \\ &+ \sum_\alpha^{N_\mathrm{freq}} \sum_\beta^{N_\mathrm{dir}} \sum_\gamma^{N_\mathrm{mode}} \mathrm{Re}\left\{ \int_{\Omega_\mathrm{cell}} \mathrm{grad}\,\overline{\mathbf{v}} : \delta_\lambda \underline{\underline{\mathbf{C}}}\left[\mathrm{grad}\,\mathbf{u}\right] d\Omega \right\} \\ &+ \sum_\alpha^{N_\mathrm{freq}} \sum_\beta^{N_\mathrm{dir}} \sum_\gamma^{N_\mathrm{mode}} \mathrm{Re}\left\{ \mathrm{i}k \int_{\Omega_\mathrm{cell}} \left\{ \mathrm{grad}\,\overline{\mathbf{v}} : \delta_\lambda \underline{\underline{\mathbf{C}}}[\mathbf{u}\otimes\mathbf{d}] - (\overline{\mathbf{v}}\otimes\mathbf{d}) : \delta_\lambda \underline{\underline{\mathbf{C}}}\left[\mathrm{grad}\,\mathbf{u}\right] \right\} d\Omega \right\} \\ &+ \sum_\alpha^{N_\mathrm{freq}} \sum_\beta^{N_\mathrm{dir}} \sum_\gamma^{N_\mathrm{mode}} \mathrm{Re}\left\{ k^2 \int_{\Omega_\mathrm{cell}} (\overline{\mathbf{v}}\otimes\mathbf{d}) : \delta_\lambda \underline{\underline{\mathbf{C}}}[\mathbf{u}\otimes\mathbf{d}] d\Omega \right\} \\ &+ \sum_\alpha^{N_\mathrm{freq}} \sum_\beta^{N_\mathrm{dir}} \sum_\gamma^{N_\mathrm{mode}} \mathrm{Re}\left\{ \frac{\xi}{2} \int_{\Omega_\mathrm{cell}} (\overline{\mathbf{v}}\otimes\mathbf{d}) : \delta_\lambda \underline{\underline{\mathbf{C}}}[\mathbf{u}\otimes\mathbf{d}] d\Omega \right\} \quad \forall \tilde{\lambda} \in \mathcal{W}, \quad \text{and} \end{aligned} \tag{27b}$$

$$\begin{aligned}\int_{\Omega_\mathrm{cell}} \tilde{\mu} g_\mu d\Omega = &\sum_\alpha^{N_\mathrm{freq}} \sum_\beta^{N_\mathrm{dir}} \sum_\gamma^{N_\mathrm{mode}} \left(-\frac{\mathrm{i}\int_{\Omega_\mathrm{cell}} \left\{ \mathrm{grad}\,\overline{\mathbf{u}} : \delta_\mu \underline{\underline{\mathbf{C}}}[\mathbf{u}\otimes\mathbf{d}] - (\overline{\mathbf{u}}\otimes\mathbf{d}) : \delta_\mu \underline{\underline{\mathbf{C}}}\left[\mathrm{grad}\,\mathbf{u}\right] \right\} d\Omega}{2\omega a_{0,2}(\mathbf{u},\mathbf{u})} \right. \\ &\left. - \frac{2\mathrm{Re}\{k\} \int_{\Omega_\mathrm{cell}} (\overline{\mathbf{u}}\otimes\mathbf{d}) : \delta_\mu \underline{\underline{\mathbf{C}}}[\mathbf{u}\otimes\mathbf{d}] d\Omega}{2\omega a_{0,2}(\mathbf{u},\mathbf{u})} \right) \left(v_g - v_g^m\right) \\ &+ \sum_\alpha^{N_\mathrm{freq}} \sum_\beta^{N_\mathrm{dir}} \sum_\gamma^{N_\mathrm{mode}} \mathrm{Re}\left\{ \int_{\Omega_\mathrm{cell}} \mathrm{grad}\,\overline{\mathbf{v}} : \delta_\mu \underline{\underline{\mathbf{C}}}\left[\mathrm{grad}\,\mathbf{u}\right] d\Omega \right\} \\ &+ \sum_\alpha^{N_\mathrm{freq}} \sum_\beta^{N_\mathrm{dir}} \sum_\gamma^{N_\mathrm{mode}} \mathrm{Re}\left\{ \mathrm{i}k \int_{\Omega_\mathrm{cell}} \left\{ \mathrm{grad}\,\overline{\mathbf{v}} : \delta_\mu \underline{\underline{\mathbf{C}}}[\mathbf{u}\otimes\mathbf{d}] - (\overline{\mathbf{v}}\otimes\mathbf{d}) : \delta_\mu \underline{\underline{\mathbf{C}}}\left[\mathrm{grad}\,\mathbf{u}\right] \right\} d\Omega \right\} \\ &+ \sum_\alpha^{N_\mathrm{freq}} \sum_\beta^{N_\mathrm{dir}} \sum_\gamma^{N_\mathrm{mode}} \mathrm{Re}\left\{ k^2 \int_{\Omega_\mathrm{cell}} (\overline{\mathbf{v}}\otimes\mathbf{d}) : \delta_\mu \underline{\underline{\mathbf{C}}}[\mathbf{u}\otimes\mathbf{d}] d\Omega \right\} \\ &+ \sum_\alpha^{N_\mathrm{freq}} \sum_\beta^{N_\mathrm{dir}} \sum_\gamma^{N_\mathrm{mode}} \mathrm{Re}\left\{ \frac{\xi}{2} \int_{\Omega_\mathrm{cell}} (\overline{\mathbf{v}}\otimes\mathbf{d}) : \delta_\mu \underline{\underline{\mathbf{C}}}[\mathbf{u}\otimes\mathbf{d}] d\Omega \right\} \quad \forall \tilde{\mu} \in \mathcal{W}, \end{aligned} \tag{27c}$$

where,

$$\delta_\lambda \underline{\underline{\mathbf{C}}}[\,] = \tilde{\lambda}\,\mathrm{tr}[\,]\underline{\mathbf{I}} \quad \text{and} \tag{28a}$$

$$\delta_\mu \underline{\underline{\mathbf{C}}}[\,] = \tilde{\mu}[\,] + \tilde{\mu}[\,]^\mathsf{T}. \tag{28b}$$

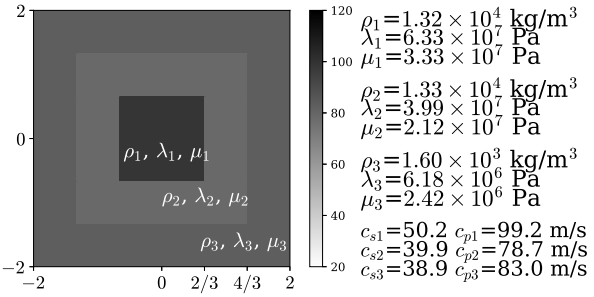

(a) Inverted unit-cell material properties

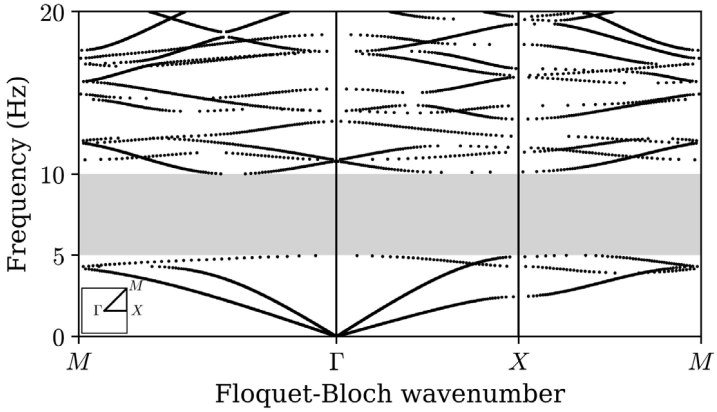

(b) Band structure along the high-symmetry lines

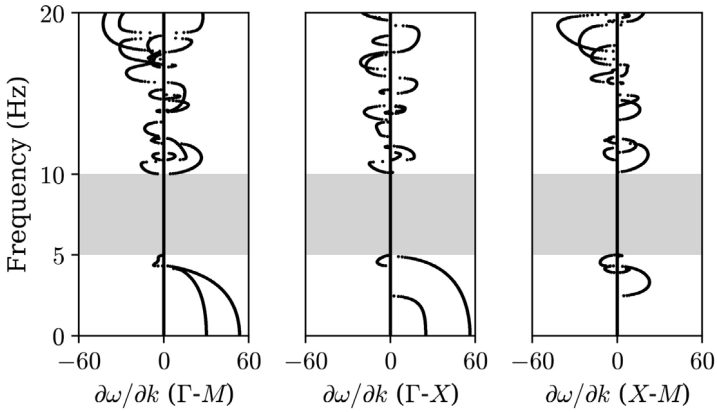

(c) Group velocity along the high-symmetry lines

Fig. 3. Unit cell design for an omnidirectional band gap at $\mathcal{G} = (5, 10)$ Hz.

The detailed derivations are provided in Appendix B. The gradients (27) vanish only at a stationary point of the Lagrangian L; they are used, in the context of a conjugate gradient method [31], in order to update the design variables. The algorithm for the inverse metamaterial design is summarized in Algorithm 1.

Algorithm 1 Inverse design process

1: Sample the target group velocity v_g^m ($v_g^m = 0$ for band gaps) at discrete frequencies, directions, and modes
2: Define the geometry of the unit cell (e.g., periodicity, number of distinct material elements, etc.)
3: Set the error tolerance ε.
4: Initialize the iteration counter $l \leftarrow 0$
5: Set the initial search length
6: Set initial guesses for the material properties ρ_0, λ_0, and μ_0
7: **for** $\|M_{l+1} - M_l\| > \varepsilon \|M_l\|$ **do**
8: Solve the state problem and evaluate M_l ▷ equations (24b) and (25)
9: Solve the adjoint problem ▷ equation (26)
10: Compute the reduced gradient of L ▷ equations (27)
11: Obtain the search direction (e.g., conjugate gradient method)
12: Update the material properties ρ_{l+1}, λ_{l+1}, and μ_{l+1} using backtracking algorithm; stop if sufficient-decrease condition is violated
13: Set $l \leftarrow l + 1$
14: **end for**

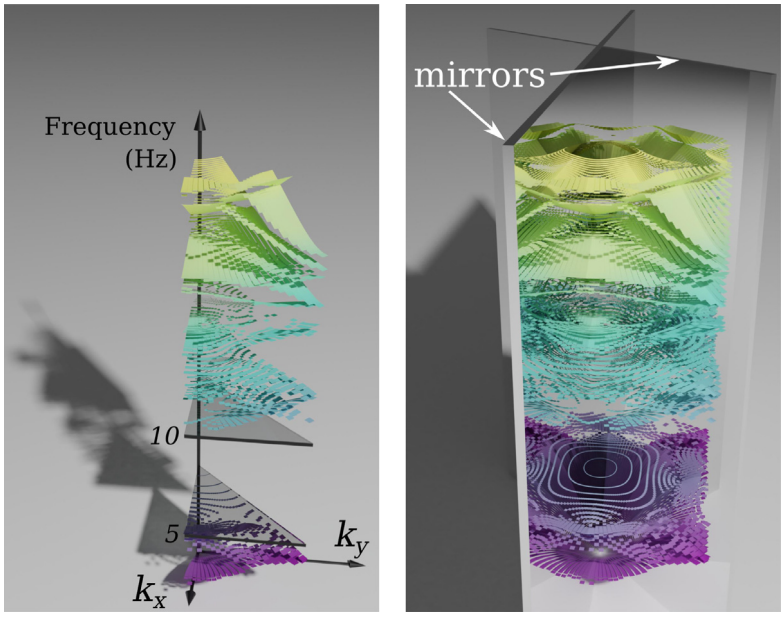

(a) Dispersion surfaces of the irreducible Brillouin zone - IBZ

(b) Dispersion surfaces of the Brillouin zone

Fig. 4. Complete band structure showing an omnidirectional target band gap at $\mathcal{G} = (5, 10)$ Hz.

4. Metamaterial band-gap design examples

The proposed design method can invert for a unit cell's properties when provided with a user-defined group velocity profile. In the following examples, we demonstrate the method by inverting for the mass density and the Lamé parameters of multi-material unit cells to effect either uni- or omnidirectional user-defined band gaps. In all cases, we use finite elements (biquadratic serendipity elements) to solve the state and adjoint problems.

An omnidirectional band gap. First, we attempt to invert for the properties of a square unit cell to effect an omnidirectional band gap at $\mathcal{G} = (5, 10)$ Hz. The unit cell consists of three concentric squares of different materials, with sides 4 m, 8/3 m, and 4/3 m, respectively (Fig. 3); the properties were seeded to $\rho_1 = 10081.370$ kg/m^3,

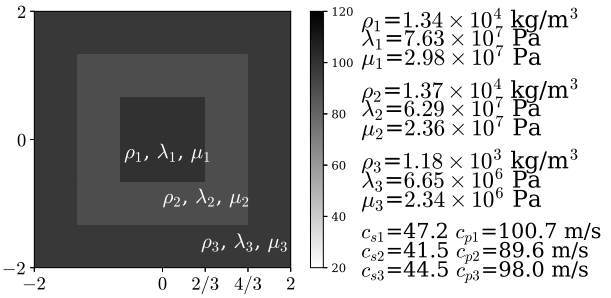

(a) Inverted unit-cell material properties

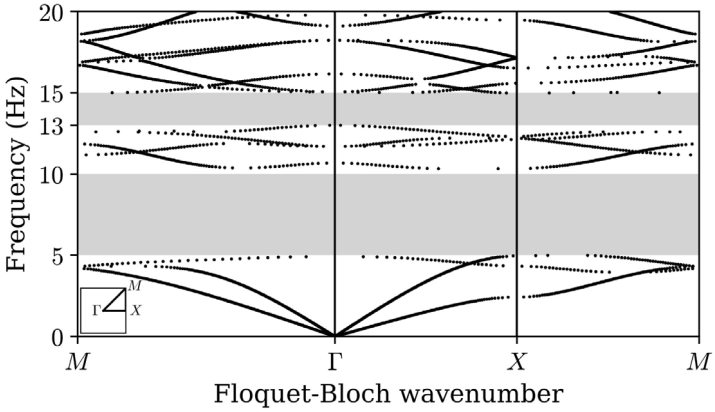

(b) Band structure along the high-symmetry lines

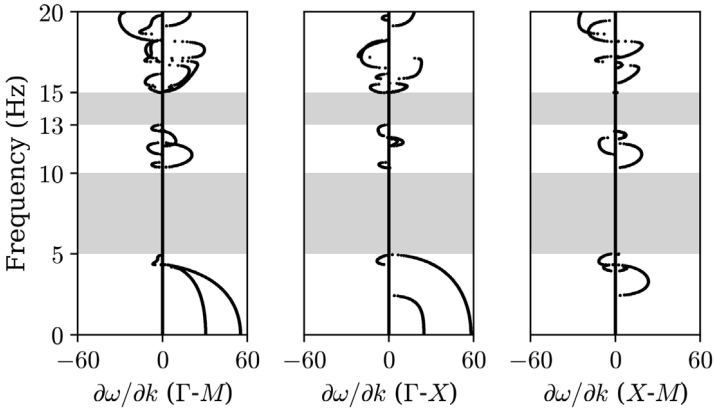

(c) Group velocity along the high-symmetry lines

Fig. 5. Unit cell design for two omnidirectional band gaps at $\mathcal{G} = (5, 10) \cup (13, 15)$ Hz.

$\lambda_1 = 63.266$ MPa, $\mu_1 = 33.266$ MPa, for the innermost square, $\rho_2 = 7730.992$ kg/m^3, $\lambda_2 = 41.213$ MPa, $\mu_2 = 21.213$ MPa, for the middle, and $\rho_3 = 73.61$ kg/m^3, $\lambda_3 = 7.443$ MPa, $\mu_3 = 3.843$ MPa for the outermost square.

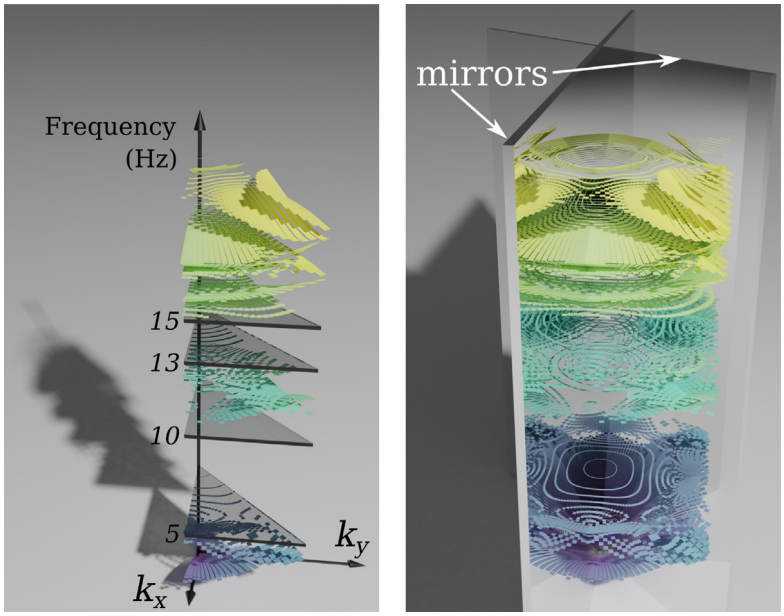

(a) Dispersion surfaces of the irreducible Brillouin zone - IBZ

(b) Dispersion surfaces of the Brillouin zone

Fig. 6. Complete band structure showing two omnidirectional band gaps at $\mathcal{G} = (5, 10) \cup (13, 15)$ Hz.

We use fifty frequencies ($N_{\text{freq}} = 50$) to span $\mathcal{G}$, and ten directions to sweep over the IBZ ($N_{\text{dir}} = 10$) in order to enforce omnidirectional behavior; the number of modes N_{mode} equals the number of wavenumbers within the first Brillouin zone, and, thus, it varies per frequency. The target group velocities for all of the N_{freq} frequencies, the N_{dir} directions, and the N_{mode} modes are set to zero, i.e., $v^m_{g,\alpha\beta\gamma} = 0$. Fig. 3(a) depicts the unit cell's converged material properties, while Fig. 3(b) and Fig. 3(c) show the band structure and group velocity profiles along the high-symmetry lines, respectively. As it can be deduced from the band structure the target band gap, shown in the figures with the shaded strip, was indeed realized (to minimize graphical congestion in the band structure, only the real-valued wavenumbers are plotted). Fig. 4 shows the complete three-dimensional dispersion surfaces in the IBZ (Fig. 4(a)), and by using graphic mirroring, in the Brillouin zone as well (Fig. 4(b)): each plane represents a single wavevector computation, the width of which is proportional to the magnitude of the wavevector, and the slope is guided by the group velocity.

Two omnidirectional band gaps. Next, we exercise the inversion algorithm by seeking a metamaterial that would simultaneously exhibit two user-defined band gaps, i.e., $\mathcal{G} = (5, 10)\,\text{Hz} \cup (13, 15)\,\text{Hz}$. We seed the inversion algorithm with the converged properties of the preceding example's unit cell. Fig. 5(a) shows the converged material profile, while Figs. 5(b) and (c) depict again the corresponding band structure and group velocity profiles, respectively. As it can be seen, the inversion algorithm successfully resulted in opening a second band gap at the target frequency range (13,15) Hz, while still maintaining the first gap at (5,10) Hz. Fig. 6 shows the metamaterial's three-dimensional dispersion map.

A unidirectional band gap at $(5, 10)$ *Hz.* Next, we target a unidirectional band gap at $(5, 10)$ Hz along Γ-X only. Fig. 7 shows that a unidirectional band gap is achieved exactly at the target frequency range. Fig. 8 shows the three-dimensional dispersion map.

5. Metabarrier time-domain performance

The preceding development is predicated upon infinite periodicity, while, in practice, one may be able to install only a finite number of unit cells in a host medium. In this section, we assess the performance of the unit cells in the

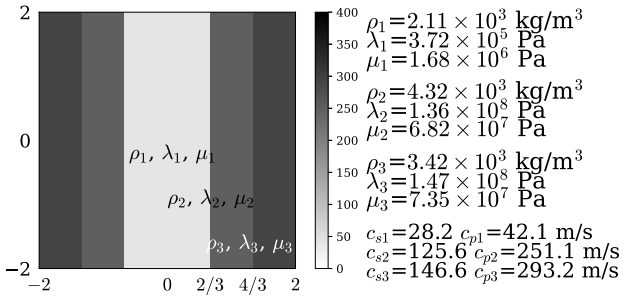

(a) Inverted unit-cell material properties

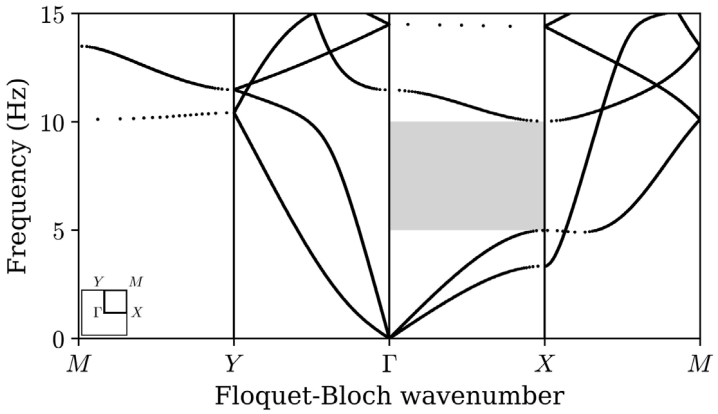

(b) Band structure along the high-symmetry lines

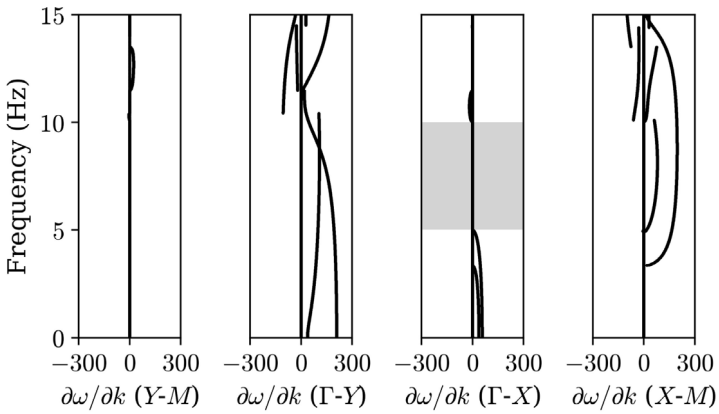

(c) Group velocity along the high-symmetry lines

Fig. 7. Unit cell design for a unidirectional band gap at $\mathcal{G} = (5, 10)$ Hz.

time-domain – where it matters most for applications – by using the inverted-for unit cells to construct finite-size metabarriers. The unit cells appear with a fairly narrow periodicity: only 2- or 4-unit-cell wide. The intent is to

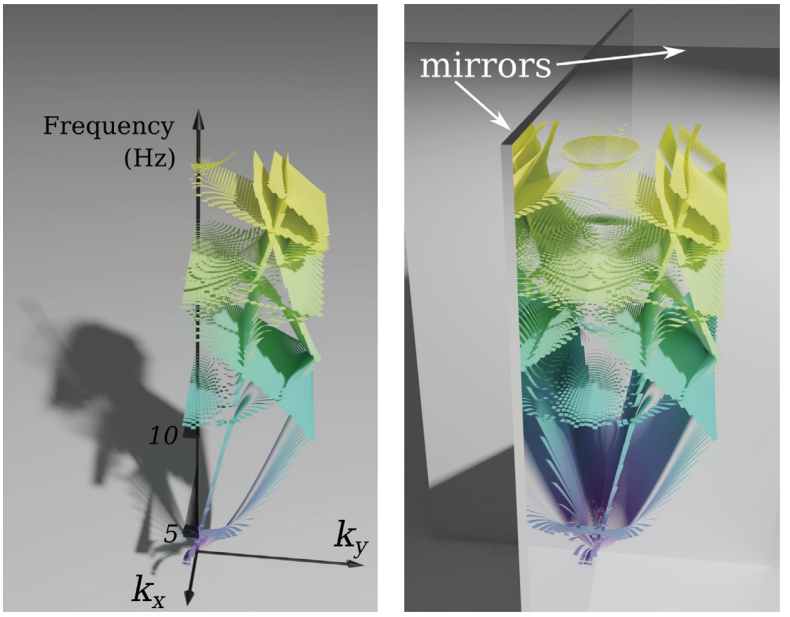

(a) Dispersion surfaces of the irreducible Brillouin zone - IBZ

(b) Dispersion surfaces of the Brillouin zone

Fig. 8. Complete band structure showing an unidirectional band gap at $\mathcal{G} = (5, 10)$ Hz.

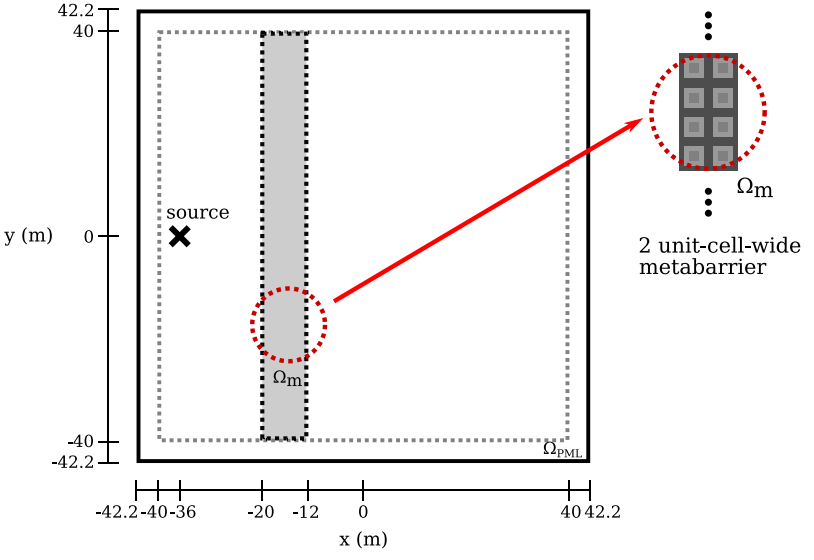

Fig. 9. Schematic of an omnidirectional P and SV metabarrier.

study via numerical simulations whether the metabarriers could still realize the directional or omnidirectional band gaps their constituent unit cells were designed for, even when the infinite periodicity assumption is violated.

An omnidirectional P and SV metabarrier. First, we discuss the P and SV omnidirectional band-gap case. As shown in Fig. 9, a two-unit-cell-wide metabarrier Ω_m is embedded within an infinite homogeneous domain truncated by Perfectly-Matched-Layers (PMLs) [32,33]. The metabarrier is constructed using the unit cell of the first design example exhibiting a band gap at $\mathcal{G} = (5, 10)$ Hz (Fig. 3). The host medium's properties are $\rho = 2000$ kg/m^3,

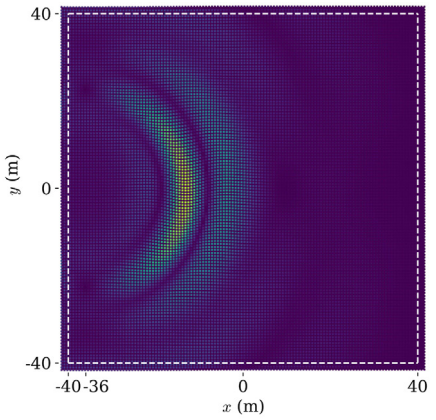

(a) Without metabarrier; snapshot at $t = 0.26$ s

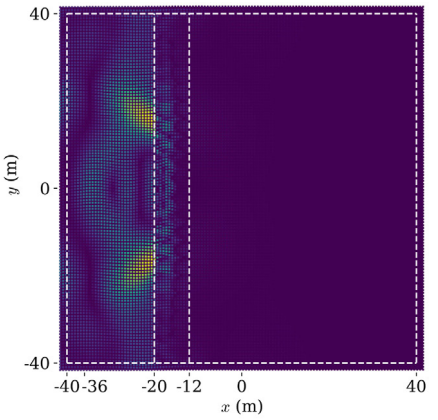

(b) With metabarrier (two-unit-cell-wide); snapshot at $t = 0.26$ s

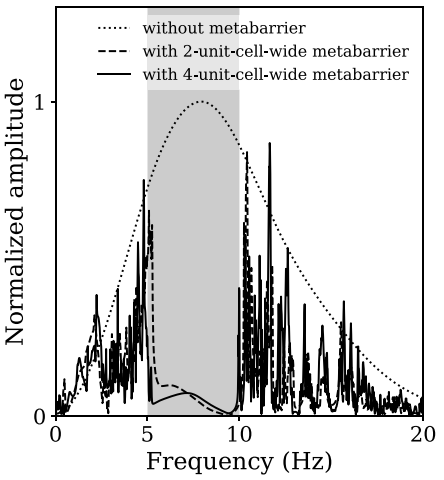

(c) DFT responses at $(x, y) = (0, 0)$ m

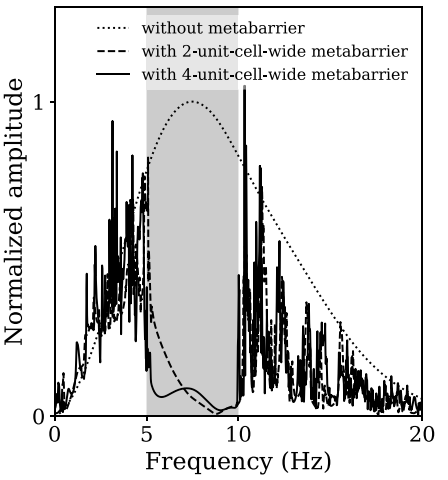

(d) DFT responses at $(x, y) = (0, 22)$ m

Fig. 10. Omnidirectional metabarrier performance: snapshots and DFT response of wavefields induced by a Ricker pulse with a central frequency of $f_c = 9$ Hz.

$\lambda = 160$ MPa, and $\mu = 80$ MPa. A Ricker pulse with a central frequency of $f_c = 9$ Hz is applied at $(x, y) = (-36, 0)$ m. The point source creates cylindrical wave fronts impinging on the metabarrier at various angles of incidence.

Fig. 10(a) and (b) depict snapshots of the displacement-field at $t = 0.26$ s for cases without and with the metabarrier, respectively. Visually, it appears that the metabarrier, despite its narrow periodicity, effectively arrested the propagation of the waves past the barrier. Fig. 10 show the response DFT at two locations past the barrier: the dotted trace corresponds to the case without the metabarrier, whereas the dashed and solid lines correspond to a two-unit-cell-wide and a four-unit-cell-wide metabarriers, respectively. The shaded strip delineates the frequency range of the design band gap: as it can be seen both barriers suppressed the motion at the band gap, as intended. Moreover, notice that even though the suppression is somewhat stronger with the four-unit-cell-wide metabarrier, the difference between the two is relatively small.

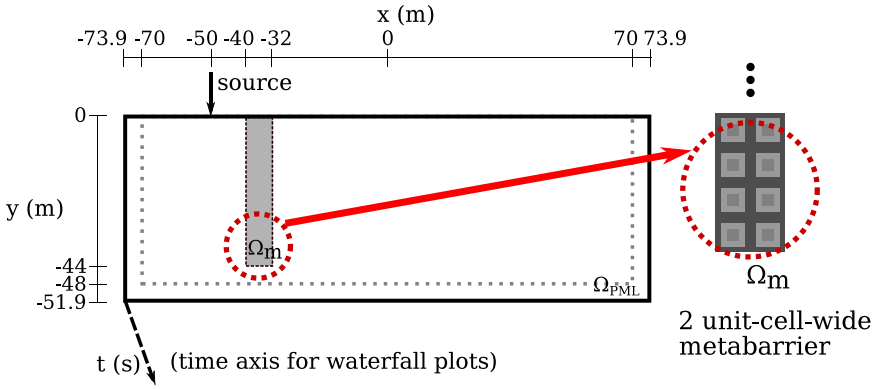

Fig. 11. Schematic of an omnidirectional vertical screen.

An omnidirectional vertical screen. We are interested in assessing whether the same finite-width engineered metabarrier of the preceding example can be used as a vertical screen in a halfspace, when the halfspace is subjected to a surficial line load in the vicinity of the screen. While the unit cell has been engineered for band-gapping P and SV waves, the line load on the halfspace's surface introduces additional waves (Rayleigh, and the S head wave) that were not accounted for in the unit-cell design. Fig. 11 captures the setting: a two-unit-cell-wide and eleven-unit-cell-long, or 44-meter-long, metabarrier is embedded in a two-dimensional semi-infinite domain truncated by PMLs. The screen's length is approximately equal to 2.2 λ_R, where λ_R denotes the Rayleigh wavelength corresponding to the surrounding medium's properties. At a depth of 2.2 λ_R, the motion amplitudes are significantly smaller than those on the surface: for example, the vertical component of the Rayleigh wave is approximately 1% of the surface amplitude, and thus the screen's length is approximately equal to the full extent of the Rayleigh wavefront. We use the unit cell of the first design example exhibiting a band gap at $\mathcal{G} = (5, 10)$ Hz to construct the metabarrier/vertical screen. A vertical line load is applied on the surface of the host medium. We visualize the response using waterfall plots, i.e., a horizontal stack of displacement-field snapshots over a time period of $t \in [0, 0.5]$ s.

Three different signals are used to exercise the screen. A monochromatic source with frequency of $f = 2.5$ Hz is used first: the frequency lies outside of the unit cell's band gap, and, thus, propagation should not be arrested. Indeed, as shown in the waterfalls of Fig. 12(a),(b), the wave front propagates unimpeded through the screen, albeit with a phase delay. By contrast, when the monochromatic source operates at 8 Hz, which lies within the design band gap, the waves are reflected by the screen, effectively arresting propagation in the forward scatter region of the screen (Fig. 12(c),(d)). Next, we apply a Ricker pulse with a central frequency of $f_c = 9$ Hz; the Ricker pulse has a broad spectrum support, roughly between 3 and 27 Hz (three times the central frequency on each side of f_c). Figs. 12(e),(f) capture the effect of the screen: as it can be seen, it appears that propagation has been arrested, as it was expected for at least the range for which the screen was designed (5 to 10 Hz).

To better quantify our observations, we compute the DFT of the response at four locations, two in the backscatter region (between the source and the metabarrier), and two in the forward scatter region of the metabarrier. In Fig. 13, figures (a) and (b) pertain to two points on the surface of the halfspace, whereas figures (c) and (d) pertain to two points at depth. For each of the four locations, four DFT curves are shown, corresponding to metabarriers of different lengths, as well as the case of the homogeneous medium without a metabarrier (black-dotted line). The three screens have lengths of 44 m (red-solid line), 20 m (blue-dash-dotted line), and 12 m (green-dashed line), respectively. The lengths correspond to depths at which the amplitude of the Rayleigh vertical component is 1%, 20%, and 50% of the amplitude on the surface, respectively.

The shaded strip in the DFT spans the design band gap: as it can be seen from the right figure-column, which corresponds to points in the forward scatter region, the 44-meter-long screen, almost perfectly, arrested propagation for frequencies within the band gap. The 20-meter-long screen also shows relatively good band-gapping performance. However, the 12-meter-long screen is less effective on the surface (still resulting in more than 50% amplitude reduction), but fails, expectedly, to arrest wave propagation at $y = -14$ m, which is located deeper than the screen. The DFT on the left column shows that there is motion amplification in the backscatter region at depth,

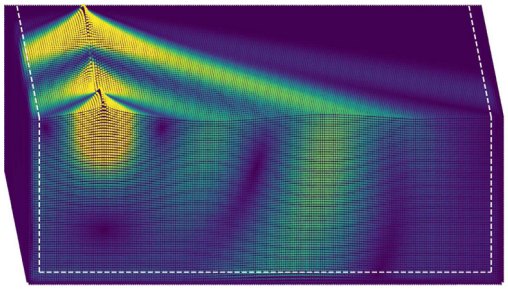

(a) Monochromatic source at $f = 2.5$ Hz $\notin \mathcal{G}$; without metabarrier

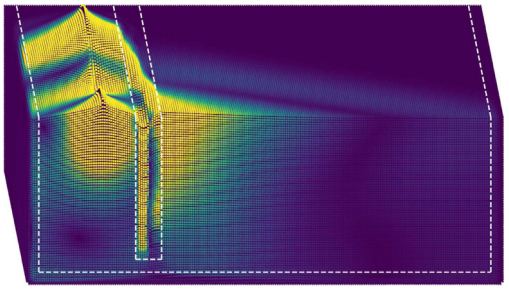

(b) Monochromatic source at $f = 2.5$ Hz $\notin \mathcal{G}$; with metabarrier (44m-long)

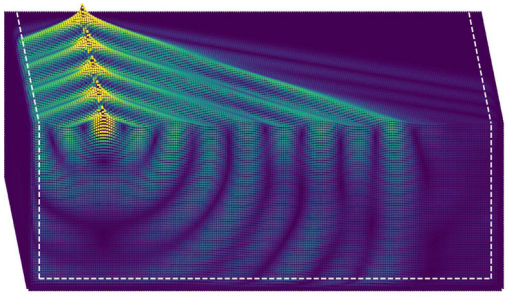

(c) Monochromatic source at $f = 8$ Hz $\in \mathcal{G}$; without metabarrier

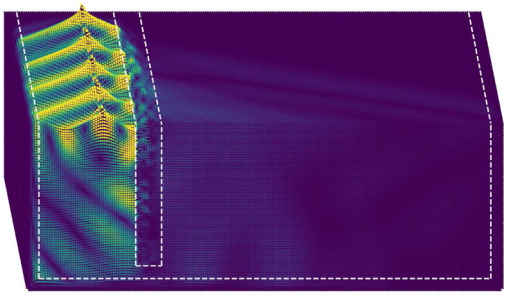

(d) Monochromatic source at $f = 8$ Hz $\in \mathcal{G}$; with metabarrier (44m-long)

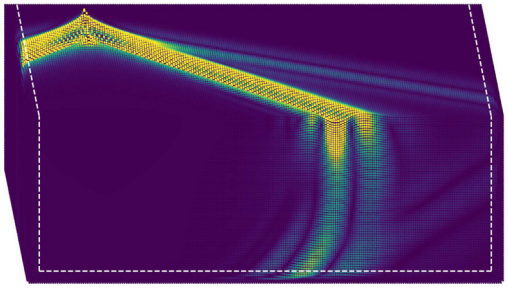

(e) Ricker pulse with $f_c = 9$ Hz; without metabarrier

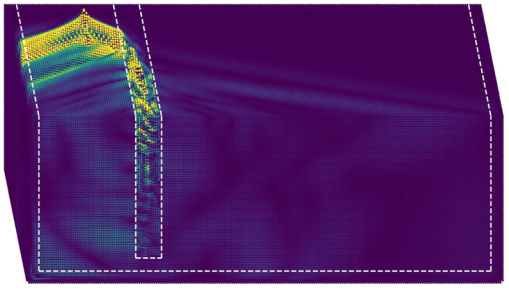

(f) Ricker pulse with $f_c = 9$ Hz; with metabarrier (44m-long)

Fig. 12. Response of an engineered vertical metabarrier to various excitations.

and, to a lesser extent, on the surface. The amplification on the surface is due to the constructive interference of the incoming motion with the waves reflected off of the metabarrier, and can be alleviated, as was shown in [24], by introducing small amount of damping in the screen.

Wave steering and shielding. Next, we turn to applications that could benefit from an omnidirectional design. First, we consider an infinite two-dimensional domain, which we truncate to a finite computational domain of 140 m $\times$ 48 m, surrounded on all sides by PMLs. We impregnate the mid half of the domain (80 m $\times$ 48 m) with the engineered unit cells (each cell is 4 m $\times$ 4 m) of the first design example, exhibiting an omnidirectional band gap at (5, 10) Hz. Then, we intentionally modify part of the metastructure, by creating a one-unit-cell-wide channel made of the same material as the infinite domain. We then trigger a point load, located in the exterior of the metastructure and in the vicinity of the channel. The generated waves impinge at various angles on the metastructure: owing to the omnidirectional band gap, the motion in the metastructure is inhibited, allowing the waves to propagate only

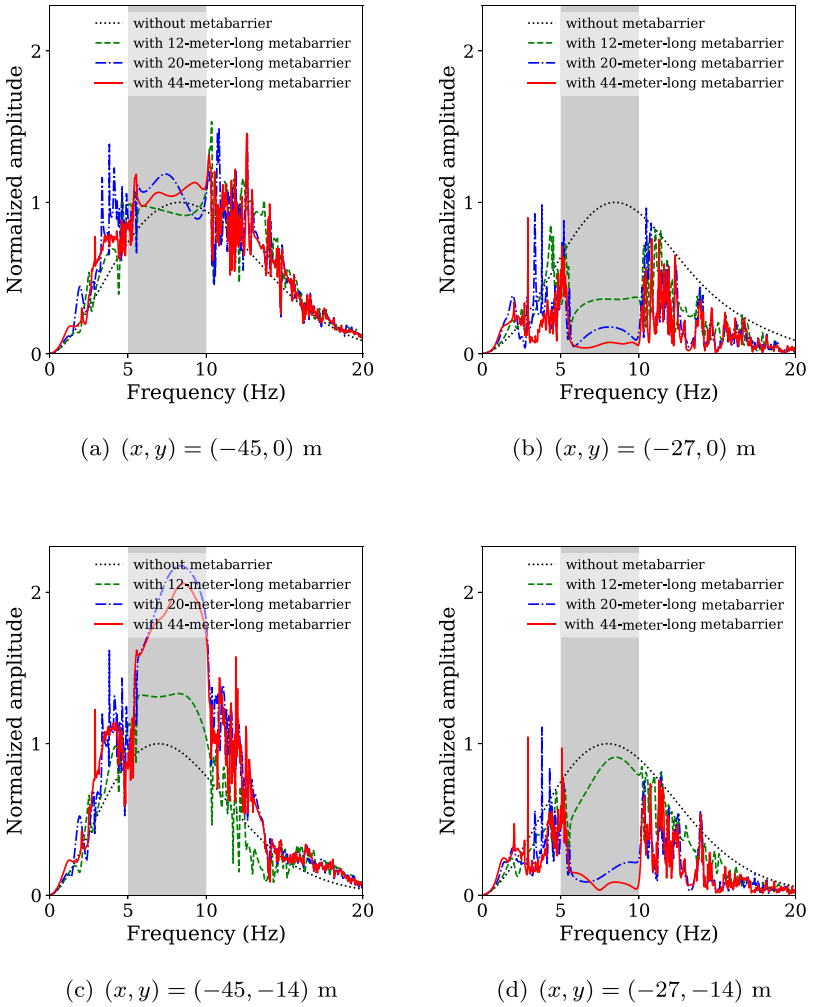

Fig. 13. DFT responses at various locations before (left column) and after (right column) the metabarrier.

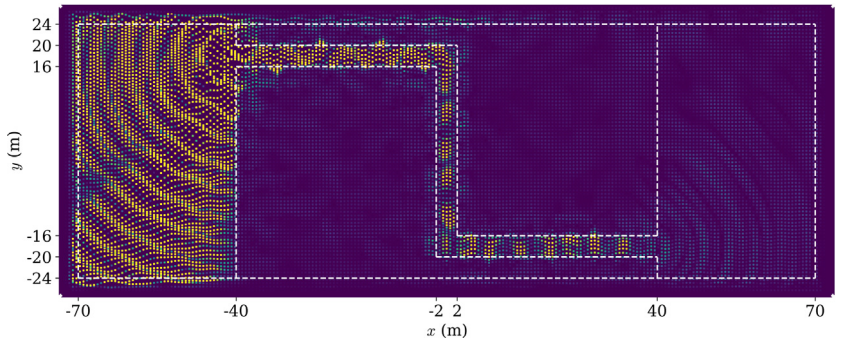

Fig. 14. Wave steering in a homogeneous medium impregnated with metamaterials.

within the channel, effectively steering the waves through the artificial waveguide. Fig. 14 shows a snapshot in time of the waveguide effect.

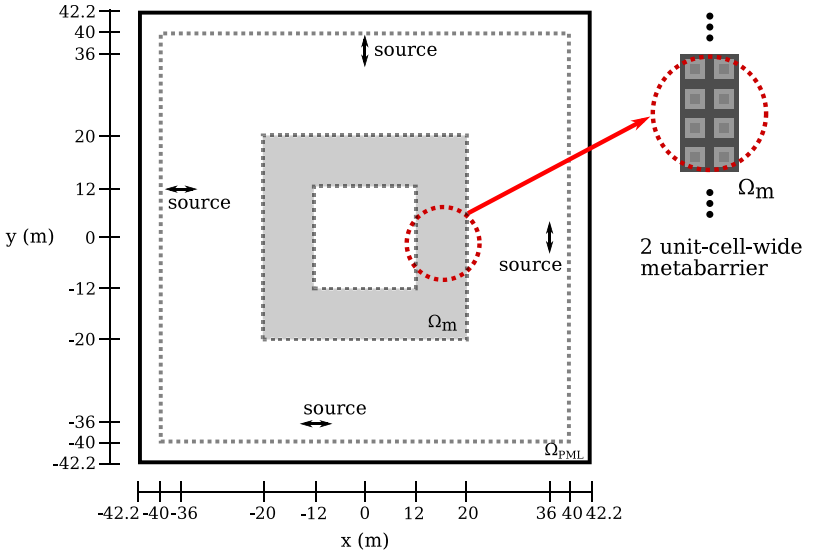

Fig. 15. Schematic of a wave shield.

Next, we use again the same unit-cell design, and create a hollow rectangle (Fig. 15) of two-unit-cell width. The intent is to examine whether the interior of the rectangle could be protected/shielded from propagating waves that originate in the exterior of the shield, and impinge, asynchronously, on the shield at various angles. To this end, we place four point sources in the exterior of the shield (Fig. 15), which are triggered at different moments in time (Ricker pulses operating at a central frequency of $f_c = 9$ Hz), along different directions (see Fig. 16).

To quantify the response of the shield, and compare it with the unshielded case, we compute the energy density E_{Ω^e}, normalized by the input energy, in order to track energy propagation within the computational domain. To this end, let:

$$E_{\Omega^e} = \frac{\frac{1}{2}\int_0^T \left\{ \int_{\Omega^e} \operatorname{grad} \mathbf{U}_t : \underline{\underline{\mathbf{C}}} \left[\operatorname{grad} \mathbf{U}_t \right] d\Omega + \int_{\Omega^e} \frac{\partial \mathbf{U}_t}{\partial t} \cdot \rho \frac{\partial \mathbf{U}_t}{\partial t} d\Omega \right\} dt}{\frac{1}{2}\int_0^T \int_{\Omega} \mathbf{f} \cdot \mathbf{U}_t \, d\Omega \, dt}, \tag{29}$$

where $\mathbf{U}_t$ is the displacement field in the time-domain, and $\mathbf{f}$ is the source. Fig. 17 depicts the energy density without and with the shield. We note the near-silent center section of the domain, attesting to the shielding efficacy of the finite metabarrier, under the asynchronous P and SV wave load impinging on the shield at arbitrary angles.

6. Conclusions

We proposed a systematic design method for engineering the dispersive properties of periodic media as a means of controlling elastic wave propagation. Specifically, we cast the design problem as a dispersion-constrained inverse problem, comprising: (a) a misfit functional between the design group velocity profile and the group velocity profile corresponding to trial design unit-cell variables, and: (b) the side-imposition of the unit-cell Floquet–Bloch eigenvalue problem. The group velocity is expressed in terms of an eigenpair, thus readily allowing the use of any standard optimization scheme to resolve the inverse problem. The proposed inverse design framework can handle various unit-cell variables, including geometric and material parameters. We demonstrated the proposed method by designing unit cells exhibiting unidirectional or omnidirectional band gaps at user-specified frequency ranges. The time-domain analyses showed that metabarriers constructed with only a few unit cells, i.e., by severely limiting the periodicity, can still harness the benefits of the engineered unit-cell dispersive behavior. We showed that the developed framework can lead to metamaterial designs capable of band-gapping, wave steering, and shielding, in the presence of both P and SV waves, and, in fact, proved effective even for surface interface waves.

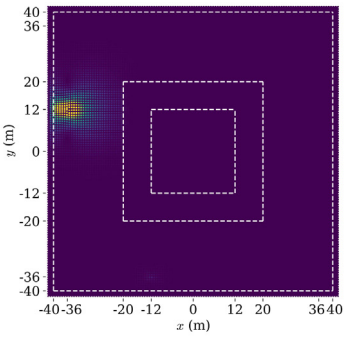

(a) West source triggered; snapshot at $t = 0.0975$ s

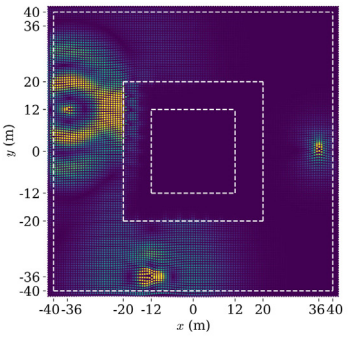

(b) South and east sources triggered; snapshot at $t = 0.1875$ s

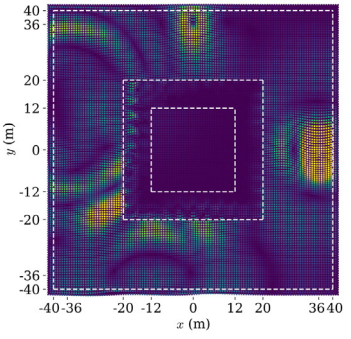

(c) All sources triggered; snapshot at $t = 0.2625$ s

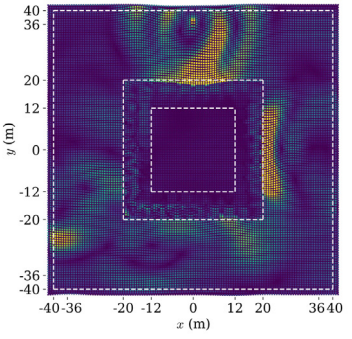

(d) Shield fully engaged; snapshot at $t = 0.3375$ s

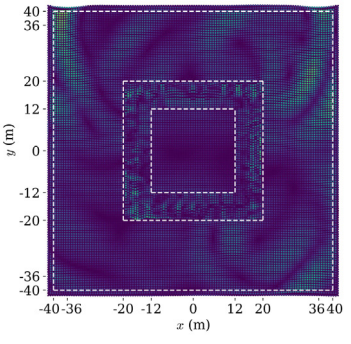

(e) Shield fully engaged; snapshot at $t = 0.4875$ s

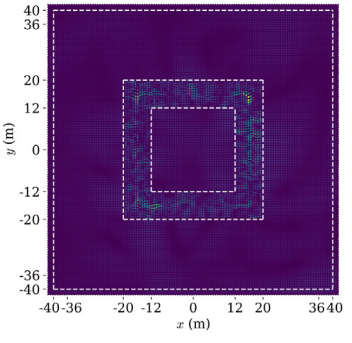

(f) Shield fully engaged; snapshot at $t = 0.8250$ s

Fig. 16. Snapshots of a wave shield's response to asynchronously triggered sources.

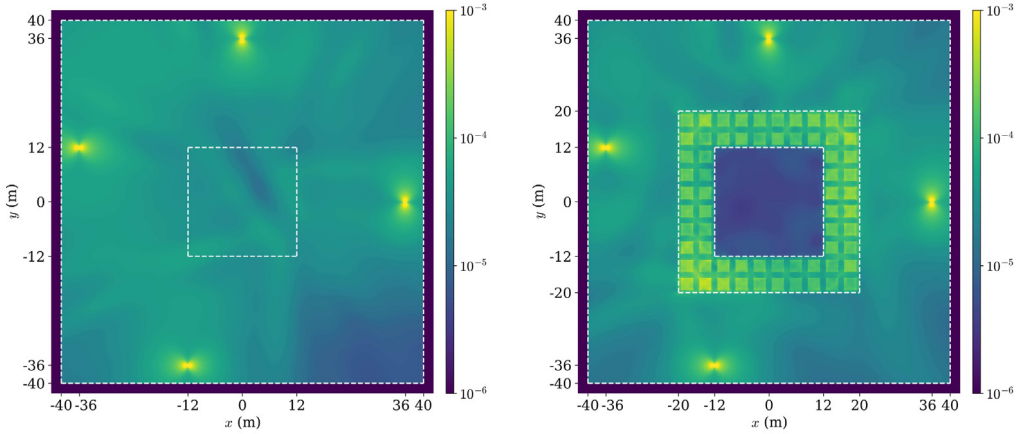

(a) Without the shield (b) With the shield

Fig. 17. Normalized energy density distribution due to four point source Ricker pulses operating at $f_c = 9$ Hz.

Declaration of competing interest

The authors declare that they have no known competing financial interests or personal relationships that could have appeared to influence the work reported in this paper.

Appendix A. Floquet–Bloch eigenvalue problem with an offset direction

A non-zero offset direction $\mathbf{d}_o$ is required for high-symmetry lines that do not connect to the origin Γ. Decomposing the Floquet–Bloch wavevector as $\mathbf{k} = k\mathbf{d} + \mathbf{d}_o$, the EP (5) is rewritten as

Given $\omega \in \mathbb{R}$, $\mathbf{d} \in \mathbb{R}^{N_\mathrm{d}}$, and $\mathbf{d}_o \in \mathbb{R}^{N_\mathrm{d}}$, find $k \in \mathbb{C}$ and $\mathbf{u} \in \mathcal{V}^{N_\mathrm{d}} \setminus \{\mathbf{0}\}$ such that

$$0 = b_0(\mathbf{v},\mathbf{u}) + k b_1(\mathbf{v},\mathbf{u}) + k^2 b_2(\mathbf{v},\mathbf{u}) \quad \forall \mathbf{v} \in \mathcal{V}^{N_\mathrm{d}}, \tag{A.1}$$

where

$$\begin{aligned} b_0(\mathbf{v},\mathbf{u}) = &\int_{\Omega_\mathrm{cell}} \left\{ \operatorname{grad}\overline{\mathbf{v}} : \underline{\underline{\mathbf{C}}}\left[\operatorname{grad}\mathbf{u}\right] - \overline{\mathbf{v}} \cdot \omega^2 \rho\, \mathbf{u} \right\} d\Omega \\ &+ \mathrm{i} \int_{\Omega_\mathrm{cell}} \left\{ \operatorname{grad}\overline{\mathbf{v}} : \underline{\underline{\mathbf{C}}}\left[\mathbf{u}\otimes\mathbf{d}_o\right] - (\overline{\mathbf{v}}\otimes\mathbf{d}_o) : \underline{\underline{\mathbf{C}}}\left[\operatorname{grad}\mathbf{u}\right] \right\} d\Omega \\ &+ \int_{\Omega_\mathrm{cell}} (\overline{\mathbf{v}}\otimes\mathbf{d}_o) : \underline{\underline{\mathbf{C}}}\left[\mathbf{u}\otimes\mathbf{d}_o\right] d\Omega, \end{aligned} \tag{A.2a}$$

$$\begin{aligned} b_1(\mathbf{v},\mathbf{u}) = &\mathrm{i} \int_{\Omega_\mathrm{cell}} \left\{ \operatorname{grad}\overline{\mathbf{v}} : \underline{\underline{\mathbf{C}}}\left[\mathbf{u}\otimes\mathbf{d}\right] - (\overline{\mathbf{v}}\otimes\mathbf{d}) : \underline{\underline{\mathbf{C}}}\left[\operatorname{grad}\mathbf{u}\right] \right\} d\Omega \\ &+ \int_{\Omega_\mathrm{cell}} \left\{ (\overline{\mathbf{v}}\otimes\mathbf{d}) : \underline{\underline{\mathbf{C}}}\left[\mathbf{u}\otimes\mathbf{d}_o\right] + (\overline{\mathbf{v}}\otimes\mathbf{d}_o) : \underline{\underline{\mathbf{C}}}\left[\mathbf{u}\otimes\mathbf{d}\right] \right\} d\Omega, \quad \text{and} \end{aligned} \tag{A.2b}$$

$$b_2(\mathbf{v},\mathbf{u}) = \int_{\Omega_\mathrm{cell}} (\overline{\mathbf{v}}\otimes\mathbf{d}) : \underline{\underline{\mathbf{C}}}\left[\mathbf{u}\otimes\mathbf{d}\right] d\Omega. \tag{A.2c}$$

For example, the directions for a two-dimensional square Brillouin zone are $\mathbf{d} = (1,0)$ and $\mathbf{d}_o = (0,0)$ for Γ-X; $\mathbf{d} = (1,1)/\sqrt{2}$ and $\mathbf{d}_o = (0,0)$ for Γ-M; and $\mathbf{d} = (0,1)$ and $\mathbf{d}_o = (\pi/p, 0)$ for X-M; where $p = |\mathbf{p}_i|$ is the width of a square unit cell.

Appendix B. The Gâteaux derivatives of the Lagrangian L

The gradient of a functional $L[\mathbf{u}]$ with respect to $\mathbf{u}$, denoted by $\mathbf{g}_u$, is defined as [34]:

$$\int_{\Omega_\mathrm{cell}} \tilde{\mathbf{u}} \cdot \mathbf{g}_u \, d\Omega = \delta_u L[\mathbf{u}](\tilde{\mathbf{u}}). \tag{B.1}$$

In the above, the Gâteaux derivative $\delta_u L\left[\mathbf{u}\right](\tilde{\mathbf{u}})$ is defined as:

$$\delta_u L\left[\mathbf{u}\right](\tilde{\mathbf{u}}) = \left.\frac{d}{d\varepsilon}\right|_{\varepsilon=0} L\left[\mathbf{u}+\varepsilon\tilde{\mathbf{u}}\right], \tag{B.2}$$

where $\tilde{\mathbf{u}}$ is a direction of the Gâteaux derivative. Then, the first-order optimality conditions read

$$\delta_v L\left[\ldots\right](\tilde{\mathbf{v}}) = 0 \quad \forall\tilde{\mathbf{v}}\in\mathcal{V}, \quad \delta_\xi L\left[\ldots\right]\left(\tilde{\xi}\right) = 0 \quad \forall\tilde{\xi}\in\mathbb{R} \tag{B.3a}$$

$$\delta_u L\left[\ldots\right](\tilde{\mathbf{u}}) = 0 \quad \forall\tilde{\mathbf{u}}\in\mathcal{V}, \quad \delta_k L\left[\ldots\right]\left(\tilde{k}\right) = 0 \quad \forall\tilde{k}\in\mathbb{C} \quad \text{and} \tag{B.3b}$$

$$\delta_\rho L\left[\ldots\right](\tilde{\rho}) = 0 \quad \forall\tilde{\rho}\in\mathcal{W}, \quad \delta_\lambda L\left[\ldots\right]\left(\tilde{\lambda}\right) = 0 \quad \forall\tilde{\lambda}\in\mathcal{W}, \quad \delta_\mu L\left[\ldots\right](\tilde{\mu}) = 0 \quad \forall\tilde{\mu}\in\mathcal{W}. \tag{B.3c}$$

In the above, $[\ldots]$ is used to abbreviate arguments. First, the Gâteaux derivatives with respect to the adjoint variables (B.3a) are:

$$\delta_v L\left[\ldots\right](\tilde{\mathbf{v}}) = \mathrm{Re}\left\{P\left(k\right)(\tilde{\mathbf{v}},\mathbf{u})\right\} \quad \text{and} \tag{B.4a}$$

$$\delta_\xi L\left[\ldots\right]\left(\tilde{\xi}\right) = \mathrm{Re}\left\{\frac{\tilde{\xi}}{2}\left[a_2\left(\mathbf{u},\mathbf{u}\right)-1\right]\right\}. \tag{B.4b}$$

Secondly, the Gâteaux derivatives with respect to the state variables (B.3b) are:

$$\delta_u L\left[\ldots\right](\tilde{\mathbf{u}}) = \delta_u M\left[\ldots\right](\tilde{\mathbf{u}}) + \delta_u E\left[\ldots\right](\tilde{\mathbf{u}}) \quad \text{and} \tag{B.5a}$$

$$\delta_k L\left[\ldots\right]\left(\tilde{k}\right) = \delta_k M\left[\ldots\right]\left(\tilde{k}\right) + \delta_k E\left[\ldots\right]\left(\tilde{k}\right), \tag{B.5b}$$

where

$$\begin{aligned}\delta_u M\left[\ldots\right](\tilde{\mathbf{u}}) = &-\frac{\mathrm{Re}\left\{a_1\left(\mathbf{u},\tilde{\mathbf{u}}\right)\right\}+2\mathrm{Re}\left\{k\right\}\mathrm{Re}\left\{a_2\left(\mathbf{u},\tilde{\mathbf{u}}\right)\right\}}{\omega a_{0,2}\left(\mathbf{u},\mathbf{u}\right)}\left(v_g-v_g^m\right)\\ &+\frac{a_1\left(\mathbf{u},\mathbf{u}\right)+2\mathrm{Re}\left\{k\right\}a_2\left(\mathbf{u},\mathbf{u}\right)}{\omega\left[a_{0,2}\left(\mathbf{u},\mathbf{u}\right)\right]^2}\mathrm{Re}\left\{a_{0,2}\left(\mathbf{u},\tilde{\mathbf{u}}\right)\right\}\left(v_g-v_g^m\right),\end{aligned} \tag{B.6a}$$

$$\delta_k M\left[\ldots\right]\left(\tilde{k}\right) = -\frac{\mathrm{Re}\left\{\tilde{k}\right\}a_2\left(\mathbf{u},\mathbf{u}\right)}{\omega a_{0,2}\left(\mathbf{u},\mathbf{u}\right)}\left(v_g-v_g^m\right), \tag{B.6b}$$

$$\delta_u E\left[\ldots\right](\tilde{\mathbf{u}}) = \mathrm{Re}\left\{P\left(k\right)(\mathbf{v},\tilde{\mathbf{u}})\right\}+\mathrm{Re}\left\{\xi a_2\left(\mathbf{u},\tilde{\mathbf{u}}\right)\right\}, \quad \text{and} \tag{B.6c}$$

$$\delta_k E\left[\ldots\right]\left(\tilde{k}\right) = \mathrm{Re}\left\{\tilde{k}a_1\left(\mathbf{v},\mathbf{u}\right)+2k\tilde{k}a_2\left(\mathbf{v},\mathbf{u}\right)\right\}. \tag{B.6d}$$

Finally, the Gâteaux derivatives with respect to the design variables (B.3c) are:

$$\delta_\rho L\left[\ldots\right](\tilde{\rho}) = \delta_\rho M\left[\ldots\right](\tilde{\rho}) + \delta_\rho E\left[\ldots\right](\tilde{\rho}), \tag{B.7a}$$

$$\delta_\lambda L\left[\ldots\right]\left(\tilde{\lambda}\right) = \delta_\lambda M\left[\ldots\right]\left(\tilde{\lambda}\right) + \delta_\lambda E\left[\ldots\right]\left(\tilde{\lambda}\right), \quad \text{and} \tag{B.7b}$$

$$\delta_\mu L\left[\ldots\right](\tilde{\mu}) = \delta_\mu M\left[\ldots\right](\tilde{\mu}) + \delta_\mu E\left[\ldots\right](\tilde{\mu}), \tag{B.7c}$$

where

$$\delta_\rho M\left[\ldots\right](\tilde{\rho}) = \sum_{\alpha}^{N_{\mathrm{freq}}}\sum_{\beta}^{N_{\mathrm{dir}}}\sum_{\gamma}^{N_{\mathrm{mode}}}\left(\frac{a_1\left(\mathbf{u},\mathbf{u}\right)+2\mathrm{Re}\left\{k\right\}a_2\left(\mathbf{u},\mathbf{u}\right)}{2\,\omega\left[a_{0,2}\left(\mathbf{u},\mathbf{u}\right)\right]^2}\right)\left(-\int_{\Omega_{\mathrm{cell}}}\overline{\mathbf{u}}\cdot\tilde{\rho}\mathbf{u}d\Omega\right)\left(v_g-v_g^m\right), \tag{B.8a}$$

$$\delta_\rho E\left[\ldots\right](\tilde{\rho}) = \sum_{\alpha}^{N_{\mathrm{freq}}}\sum_{\beta}^{N_{\mathrm{dir}}}\sum_{\gamma}^{N_{\mathrm{mode}}}\mathrm{Re}\left\{-\int_{\Omega_{\mathrm{cell}}}\overline{\mathbf{v}}\cdot\tilde{\rho}\,\omega^2\mathbf{u}d\Omega\right\}, \tag{B.8b}$$

$$\delta_\lambda M\left[\ldots\right]\left(\tilde{\lambda}\right) = \sum_{\alpha}^{N_{\text{freq}}}\sum_{\beta}^{N_{\text{dir}}}\sum_{\gamma}^{N_{\text{mode}}}\left(-\frac{\mathrm{i}\int_{\Omega_{\text{cell}}}\left\{\operatorname{grad}\overline{\mathbf{u}}:\delta_\lambda\underline{\underline{\mathbf{C}}}\left[\mathbf{u}\otimes\mathbf{d}\right]-\left(\overline{\mathbf{u}}\otimes\mathbf{d}\right):\delta_\lambda\underline{\underline{\mathbf{C}}}\left[\operatorname{grad}\mathbf{u}\right]\right\}d\Omega}{2\,\omega\,a_{0,2}\left(\mathbf{u},\mathbf{u}\right)}\right.$$
$$\left.-\frac{2\mathrm{Re}\left\{k\right\}\int_{\Omega_{\text{cell}}}\left(\overline{\mathbf{u}}\otimes\mathbf{d}\right):\delta_\lambda\underline{\underline{\mathbf{C}}}\left[\mathbf{u}\otimes\mathbf{d}\right]d\Omega}{2\,\omega\,a_{0,2}\left(\mathbf{u},\mathbf{u}\right)}\right)\left(v_g-v_g^m\right), \tag{B.8c}$$

$$\delta_\lambda E\left[\ldots\right]\left(\tilde{\lambda}\right) = \sum_{\alpha}^{N_{\text{freq}}}\sum_{\beta}^{N_{\text{dir}}}\sum_{\gamma}^{N_{\text{mode}}}\mathrm{Re}\left\{\int_{\Omega_{\text{cell}}}\operatorname{grad}\overline{\mathbf{v}}:\delta_\lambda\underline{\underline{\mathbf{C}}}\left[\operatorname{grad}\mathbf{u}\right]d\Omega\right\}$$
$$+\sum_{\alpha}^{N_{\text{freq}}}\sum_{\beta}^{N_{\text{dir}}}\sum_{\gamma}^{N_{\text{mode}}}\mathrm{Re}\left\{\mathrm{i}k\int_{\Omega_{\text{cell}}}\left\{\operatorname{grad}\overline{\mathbf{v}}:\delta_\lambda\underline{\underline{\mathbf{C}}}\left[\mathbf{u}\otimes\mathbf{d}\right]-\left(\overline{\mathbf{v}}\otimes\mathbf{d}\right):\delta_\lambda\underline{\underline{\mathbf{C}}}\left[\operatorname{grad}\mathbf{u}\right]\right\}d\Omega\right\}$$
$$+\sum_{\alpha}^{N_{\text{freq}}}\sum_{\beta}^{N_{\text{dir}}}\sum_{\gamma}^{N_{\text{mode}}}\mathrm{Re}\left\{k^2\int_{\Omega_{\text{cell}}}\left(\overline{\mathbf{v}}\otimes\mathbf{d}\right):\delta_\lambda\underline{\underline{\mathbf{C}}}\left[\mathbf{u}\otimes\mathbf{d}\right]d\Omega\right\}$$
$$+\sum_{\alpha}^{N_{\text{freq}}}\sum_{\beta}^{N_{\text{dir}}}\sum_{\gamma}^{N_{\text{mode}}}\mathrm{Re}\left\{\frac{\xi}{2}\int_{\Omega_{\text{cell}}}\left(\overline{\mathbf{v}}\otimes\mathbf{d}\right):\delta_\lambda\underline{\underline{\mathbf{C}}}\left[\mathbf{u}\otimes\mathbf{d}\right]d\Omega\right\}, \tag{B.8d}$$

$$\delta_\mu M\left[\ldots\right]\left(\tilde{\mu}\right) = \sum_{\alpha}^{N_{\text{freq}}}\sum_{\beta}^{N_{\text{dir}}}\sum_{\gamma}^{N_{\text{mode}}}\left(-\frac{\mathrm{i}\int_{\Omega_{\text{cell}}}\left\{\operatorname{grad}\overline{\mathbf{u}}:\delta_\mu\underline{\underline{\mathbf{C}}}\left[\mathbf{u}\otimes\mathbf{d}\right]-\left(\overline{\mathbf{u}}\otimes\mathbf{d}\right):\delta_\mu\underline{\underline{\mathbf{C}}}\left[\operatorname{grad}\mathbf{u}\right]\right\}d\Omega}{2\,\omega\,a_{0,2}\left(\mathbf{u},\mathbf{u}\right)}\right.$$
$$\left.-\frac{2\mathrm{Re}\left\{k\right\}\int_{\Omega_{\text{cell}}}\left(\overline{\mathbf{u}}\otimes\mathbf{d}\right):\delta_\mu\underline{\underline{\mathbf{C}}}\left[\mathbf{u}\otimes\mathbf{d}\right]d\Omega}{2\,\omega\,a_{0,2}\left(\mathbf{u},\mathbf{u}\right)}\right)\left(v_g-v_g^m\right), \quad \text{and} \tag{B.8e}$$

$$\delta_\mu E\left[\ldots\right]\left(\tilde{\mu}\right) = \sum_{\alpha}^{N_{\text{freq}}}\sum_{\beta}^{N_{\text{dir}}}\sum_{\gamma}^{N_{\text{mode}}}\mathrm{Re}\left\{\int_{\Omega_{\text{cell}}}\operatorname{grad}\overline{\mathbf{v}}:\delta_\mu\underline{\underline{\mathbf{C}}}\left[\operatorname{grad}\mathbf{u}\right]d\Omega\right\}$$
$$+\sum_{\alpha}^{N_{\text{freq}}}\sum_{\beta}^{N_{\text{dir}}}\sum_{\gamma}^{N_{\text{mode}}}\mathrm{Re}\left\{\mathrm{i}k\int_{\Omega_{\text{cell}}}\left\{\operatorname{grad}\overline{\mathbf{v}}:\delta_\mu\underline{\underline{\mathbf{C}}}\left[\mathbf{u}\otimes\mathbf{d}\right]-\left(\overline{\mathbf{v}}\otimes\mathbf{d}\right):\delta_\mu\underline{\underline{\mathbf{C}}}\left[\operatorname{grad}\mathbf{u}\right]\right\}d\Omega\right\}$$
$$+\sum_{\alpha}^{N_{\text{freq}}}\sum_{\beta}^{N_{\text{dir}}}\sum_{\gamma}^{N_{\text{mode}}}\mathrm{Re}\left\{k^2\int_{\Omega_{\text{cell}}}\left(\overline{\mathbf{v}}\otimes\mathbf{d}\right):\delta_\mu\underline{\underline{\mathbf{C}}}\left[\mathbf{u}\otimes\mathbf{d}\right]d\Omega\right\}$$
$$+\sum_{\alpha}^{N_{\text{freq}}}\sum_{\beta}^{N_{\text{dir}}}\sum_{\gamma}^{N_{\text{mode}}}\mathrm{Re}\left\{\frac{\xi}{2}\int_{\Omega_{\text{cell}}}\left(\overline{\mathbf{v}}\otimes\mathbf{d}\right):\delta_\mu\underline{\underline{\mathbf{C}}}\left[\mathbf{u}\otimes\mathbf{d}\right]d\Omega\right\}. \tag{B.8f}$$

In the above, we used:

$$\delta_\lambda\underline{\underline{\mathbf{C}}}\left[\ \right] = \tilde{\lambda}\,\mathrm{tr}\left[\ \right]\underline{\mathbf{I}} \quad \text{and} \tag{B.9a}$$
$$\delta_\mu\underline{\underline{\mathbf{C}}}\left[\ \right] = \tilde{\mu}\left[\ \right] + \tilde{\mu}\left[\ \right]^{\mathsf{T}}. \tag{B.9b}$$

References

[1] J. Pendry, A. Aubry, D. Smith, S. Maier, Transformation optics and subwavelength control of light, Science 337 (6094) (2012) 549–552.

[2] X. Su, Z. Lu, A.N. Norris, Elastic metasurfaces for splitting SV- and P-waves in elastic solids, J. Appl. Phys. 123 (9) (2018) 091701, http://dx.doi.org/10.1063/1.5007731.

[3] A. Alù, N. Engheta, Achieving transparency with plasmonic and metamaterial coatings, Phys. Rev. E 72 (1) (2005) 016623.

[4] D. Schurig, J.J. Mock, B.J. Justice, S.A. Cummer, J.B. Pendry, A.F. Starr, D.R. Smith, Metamaterial electromagnetic cloak at microwave frequencies, Science 314 (5801) (2006) 977–980.

[5] A.N. Norris, Acoustic cloaking theory, in: Proceedings of the Royal Society of London A: Mathematical, Physical and Engineering Sciences, Vol. 464, The Royal Society, 2008, pp. 2411–2434.
[6] C. Poulton, A. Movchan, R. McPhedran, N. Nicorovici, Y. Antipov, Eigenvalue problems for doubly periodic elastic structures and phononic band gaps, Proc. R. Soc. Lond. Ser. A Math. Phys. Eng. Sci. 456 (2002) (2000) 2543–2559.
[7] J.B. Pendry, Negative refraction makes a perfect lens, Phys. Rev. Lett. 85 (2000) 3966–3969, http://dx.doi.org/10.1103/PhysRevLett.85.3966.
[8] C. Luo, S.G. Johnson, J.D. Joannopoulos, J.B. Pendry, Subwavelength imaging in photonic crystals, Phys. Rev. B 68 (2003) 045115, http://dx.doi.org/10.1103/PhysRevB.68.045115.
[9] O. Sigmund, J. Søndergaard Jensen, Systematic design of phononic band–gap materials and structures by topology optimization, Philos. Trans. R. Soc. Lond. A Math. Phys. Eng. Sci. 361 (1806) (2003) 1001–1019, http://dx.doi.org/10.1098/rsta.2003.1177.
[10] X. Qian, O. Sigmund, Isogeometric shape optimization of photonic crystals via Coons patches, Comput. Methods Appl. Mech. Engrg. 200 (25) (2011) 2237–2255, http://dx.doi.org/10.1016/j.cma.2011.03.007.
[11] H. Ronellenfitsch, N. Stoop, J. Yu, A. Forrow, J. Dunkel, Inverse design of discrete mechanical metamaterials, Phys. Rev. Mater. 3 (2019) 095201, http://dx.doi.org/10.1103/PhysRevMaterials.3.095201.
[12] X. Han, Z. Zhang, Bandgap design of three-phase phononic crystal by topological optimization, Wave Motion 93 (2020) 102496, http://dx.doi.org/10.1016/j.wavemoti.2019.102496.
[13] P. Packo, A.N. Norris, D. Torrent, Inverse grating problem: Efficient design of anomalous flexural wave reflectors and refractors, Phys. Rev. Appl. 11 (2019) 014023, http://dx.doi.org/10.1103/PhysRevApplied.11.014023.
[14] B. Ahn, H. Lee, J.S. Lee, Y.Y. Kim, Topology optimization of metasurfaces for anomalous reflection of longitudinal elastic waves, Comput. Methods Appl. Mech. Engrg. 357 (2019) 112582, http://dx.doi.org/10.1016/j.cma.2019.112582.
[15] J. Gao, H. Xue, L. Gao, Z. Luo, Topology optimization for auxetic metamaterials based on isogeometric analysis, Comput. Methods Appl. Mech. Engrg. 352 (2019) 211–236, http://dx.doi.org/10.1016/j.cma.2019.04.021.
[16] G. Zhang, K. Khandelwal, Computational design of finite strain auxetic metamaterials via topology optimization and nonlinear homogenization, Comput. Methods Appl. Mech. Engrg. 356 (2019) 490–527, http://dx.doi.org/10.1016/j.cma.2019.07.027.
[17] J. Rong, W. Ye, Topology optimization design scheme for broadband non-resonant hyperbolic elastic metamaterials, Comput. Methods Appl. Mech. Engrg. 344 (2019) 819–836, http://dx.doi.org/10.1016/j.cma.2018.10.034.
[18] Y. Noguchi, T. Yamada, K. Izui, S. Nishiwaki, Topology optimization for hyperbolic acoustic metamaterials using a high-frequency homogenization method, Comput. Methods Appl. Mech. Engrg. 335 (2018) 419–471, http://dx.doi.org/10.1016/j.cma.2018.02.031.
[19] A. Asadpoure, M. Tootkaboni, L. Valdevit, Topology optimization of multiphase architected materials for energy dissipation, Comput. Methods Appl. Mech. Engrg. 325 (2017) 314–329, http://dx.doi.org/10.1016/j.cma.2017.07.007.
[20] H. Deng, L. Cheng, X. Liang, D. Hayduke, A.C. To, Topology optimization for energy dissipation design of lattice structures through snap-through behavior, Comput. Methods Appl. Mech. Engrg. 358 (2020) 112641, http://dx.doi.org/10.1016/j.cma.2019.112641.
[21] C.J. Rupp, A. Evgrafov, K. Maute, M.L. Dunn, Design of phononic materials/structures for surface wave devices using topology optimization, Struct. Multidiscip. Optim. 34 (2) (2007) 111–121, http://dx.doi.org/10.1007/s00158-006-0076-0.
[22] G. Biros, L.F. Kallivokas, S.-W. Na, Distributed parameter control of a 2D acoustic Helmholtz problem on a halfspace, in: XXI International Conference on Theoretical and Applied Mechanics (ICTAM04) - Special Sessions on Acoustics, 2004.
[23] H. Goh, L.F. Kallivokas, Inverse metamaterial design for controlling band gaps in scalar wave problems, Wave Motion 88 (2019) 85–105, http://dx.doi.org/10.1016/j.wavemoti.2019.02.001.
[24] H. Goh, L.F. Kallivokas, Group velocity-driven inverse metamaterial design, J. Eng. Mech. 145 (12) (2019) 04019094, http://dx.doi.org/10.1061/(ASCE)EM.1943-7889.0001688.
[25] N.W. Ashcroft, Solid State Physics, Holt, Rinehart and Winston, 1976, p. 403.
[26] R.P. Moiseyenko, V. Laude, Material loss influence on the complex band structure and group velocity in phononic crystals, Phys. Rev. B 83 (2011) 064301, http://dx.doi.org/10.1103/PhysRevB.83.064301.
[27] J. Willis, Negative refraction in a laminate, J. Mech. Phys. Solids 97 (2016) 10–18, http://dx.doi.org/10.1016/j.jmps.2015.11.004, SI:Pierre Suquet Symposium.
[28] V. Červený, I. Pšenčík, Energy flux in viscoelastic anisotropic media, Geophys. J. Int. 166 (3) (2006) 1299–1317, http://dx.doi.org/10.1111/j.1365-246X.2006.03057.x.
[29] K.J. Langenberg, R. Marklein, K. Mayer, Energy vs. group velocity for elastic waves in homogeneous anisotropic solid media, in: 2010 URSI International Symposium on Electromagnetic Theory, 2010, pp. 733–736, http://dx.doi.org/10.1109/URSI-EMTS.2010.5637253.
[30] M.E. Gurtin, E. Fried, L. Anand, The Mechanics and Thermodynamics of Continua, Cambridge University Press, 2010.
[31] A. Quarteroni, R. Sacco, F. Saleri, Numerical Mathematics, Vol. 37, Springer Science & Business Media, 2010, http://dx.doi.org/10.1007/b98885.
[32] S. Kucukcoban, L. Kallivokas, A symmetric hybrid formulation for transient wave simulations in pml-truncated heterogeneous media, Wave Motion 50 (1) (2013) 57–79, http://dx.doi.org/10.1016/j.wavemoti.2012.06.004.
[33] A. Fathi, B. Poursartip, L.F. Kallivokas, Time-domain hybrid formulations for wave simulations in three-dimensional pml-truncated heterogeneous media, Internat. J. Numer. Methods Engrg. 101 (3) (2015) 165–198, http://dx.doi.org/10.1002/nme.4780.
[34] M. Stone, P. Goldbart, Mathematics for Physics: a Guided Tour for Graduate Students, Cambridge University Press, 2009.